

Quantum Simulation of Light-Front QCD for Jet Quenching in Nuclear Environments

Xiaojun Yao

Center for Theoretical Physics, Massachusetts Institute of Technology, Cambridge, MA 02139 USA

E-mail: xjyao@mit.edu

ABSTRACT: We develop a framework to simulate jet quenching in nuclear environments on a quantum computer. The formulation is based on the light-front Hamiltonian dynamics of QCD. The Hamiltonian consists of three parts relevant for jet quenching studies: kinetic, diffusion and splitting terms. In the basis made up of n -particle states in momentum space, the kinetic Hamiltonian is diagonal. Matrices representing the diffusion and splitting parts are sparse. The diffusion part of the Hamiltonian depends on classical background gauge fields, which need to be sampled classically before constructing quantum circuits for the time evolution. The cost of the sampling scales linearly with the time length of the evolution and the momentum grid volume. The framework automatically keeps track of quantum interference and thus it can be applied to study the Landau-Pomeranchuk-Migdal effect in cases with more than two splittings, which is beyond the scope of state-of-the-art analyses, no matter whether the medium is static or expanding, thin or thick, hot or cold. We apply this framework to study a toy model and carry out the quantum simulation by using the IBM Qiskit simulator. The Landau-Pomeranchuk-Migdal effect that suppresses the total radiation probability is observed in the quantum simulation results.

Contents

1	Introduction	1
2	Formalism	4
2.1	Light-Front Hamiltonian Dynamics	6
2.2	Hilbert Space	8
2.3	State Initialization and Measurement	10
3	Matrix Elements of the Light-Front Hamiltonian of QCD	11
3.1	Kinetic Term	11
3.2	Diffusion Term	12
3.3	Splitting Term	16
3.4	Sampling Classical Background Field	17
4	Quantum Simulation of Toy Model	19
4.1	Toy Model	19
4.2	Construction of Quantum Circuit	20
4.2.1	Kinetic Term	22
4.2.2	Diffusion	23
4.2.3	Splitting	24
4.3	Simulation Results	25
5	Conclusions	27
A	Light-Front Hamiltonian of QCD	28
A.1	Fermion Sector	29
A.2	Gauge Sector	32
A.3	Splitting	34
B	Phase Kickback Method	35

1 Introduction

In high energy collisions, partons of large virtuality are produced from hard scatterings, which then radiate and hadronize subsequently, forming collimated sprays of particles called jets. Studying jet production can deepen our understanding of both perturbative and non-perturbative aspects of Quantum Chromodynamics (QCD), which is the theory for strong interaction in the Standard Model. In recent years, jet and jet substructure observables in proton-proton collisions have been intensively investigated in both theory and experiment [1–37].

In heavy ion collisions, jets serve as useful probes of the quark-gluon plasma (QGP), a strongly coupled fluid produced shortly after the collision. High energy partons with large virtuality are produced even earlier, much before the formation of the QGP close to thermal equilibrium. The initial hard production of partons is followed by subsequent parton showers and when the produced partons traverse the QGP, further radiation induced by the medium can happen. Eventually partons hadronize into particles at the freezeout. By comparing jets produced in proton-proton and heavy ion collisions, we are able to learn how the QGP modifies the parton shower. Jets can be thought of as external to the QGP, since the large energy scale involved in the jet production is much bigger than the typical temperature of the QGP fireball, which falls in the range $\sim [150, 600]$ MeV. In this sense, a jet can also be treated as an open quantum system embedded in the QGP fireball [38, 39]. Nevertheless, the soft ingredients of jets cannot be fully distinguished from the QGP fireball in general.

To understand and interpret experimentally measured jet and jet substructure observables in heavy ion collisions, at least three aspects of jet-medium dynamics need theoretical studies: jet energy loss, medium response and selection bias. First, when high energy partons traverse the QGP, they interact with the soft medium and as a result lose energy and momentum. This is the original idea of jet quenching in heavy ion collisions. Furthermore, the lost energy and momentum evolve in the QGP fireball, which may or may not thermalize completely to become part of the QGP, and eventually turn into particles that still have some correlation with the original high energy partons losing energy and momentum. Due to the remaining correlation, some of the particles produced in this way are reconstructed as part of the final jets. Finally, since jets of wider opening angles lose more energy than those with narrower opening angles, when experimentalists reconstruct jets of a given energy or transverse momentum, more narrower jets are selected due to the power-law decrease in jet spectra. Jet energy loss has been studied widely for a long time, while in recent years, more studies focused on understanding medium response [40–63] and selection bias [64].

Jet energy loss has been studied in both the strong coupling [65–72] and weak coupling limits. In the weak coupling (perturbative) approach, an important quantum interference effect needs consideration is called the Landau-Pomeranchuk-Migdal (LPM) effect. The LPM effect suppresses in-medium radiation because of the destructive quantum interference, caused by soft momentum exchange with the medium that modifies the phase in the time evolution in a random way. Early perturbative studies of the LPM effect focused on the case with a static medium and just one splitting, i.e., with one incoming parton and two outgoing partons for an initial quark state [73–82], and were later generalized for an incoming gluon [83–91] and expanding media [92, 93]. The difficulty of analyzing the LPM effect lies in that the soft momentum transfer from the medium and the parton splitting do not commute, which requires one to keep track of both in a time-ordered way. The soft momentum exchange process in the time evolution can be analyzed by studying a time evolution equation for a two-point correlation function, which describes the propagation of a single parton in the medium, undergoing transverse momentum broadening due to diffusion. The soft momentum exchange is encoded in terms of a “potential” term in the equation, which can be calculated in the opacity expansion or modeled. The description of the soft

momentum exchange can be improved by expanding the “potential” term perturbatively at high frequency on top of a harmonic oscillator form [94, 95]. Recent studies have attempted to investigate cases with two splittings [96–98], but the analysis becomes extremely complicated due to multiple interfering diagrams with overlapped formation times of daughter partons. Therefore, it is extremely challenging to analyze the LPM effect for cases with more than two splittings, especially when the medium is time dependent.

In this paper, we propose a framework for quantum simulation of jet quenching in hot and/or dense nuclear environments. Quantum simulation of quantum dynamics has been proposed long time ago [99] and is developing rapidly in recent years [100–116]. For applications in quantum field theory, it has been shown that scalar field theory with the $\phi^4(x)$ interaction can be efficiently simulated on a quantum computer [117–120]. Later studies investigated fermionic fields [121] and gauge theories in low dimensions [122–130]. Quantum simulation has been explored to study open quantum systems in heavy ion collisions such as heavy quarks and jets [131, 132]. Furthermore, hadron structure can also be studied on a quantum computer by using basis light-front quantization approach [133]. In the noisy intermediate-scale quantum (NISQ) era [134], error mitigation techniques [135, 136] are crucial for useful applications of quantum computers.

To simulate jet quenching on a quantum computer, we will apply the light-front Hamiltonian formulation of QCD [137] to describe the in-medium time evolution of high energy partons. The Hamiltonian relevant for jet quenching can be decomposed into three parts: a kinetic term for the phase change in the time evolution, a diffusion term accounting for the transverse momentum broadening due to the soft kicks from the medium, and a splitting term that governs radiation of partons and their recombination. The random transverse momentum exchange between the partons and the medium can be described by an external classical background gauge field that satisfies certain correlations. These correlation functions depend on the medium properties such as its temperature. The classical background field results in a random change of the kinetic energy, which leads to a random phase in the time evolution and is the crucial part for the destructive interference in the LPM effect. The classical background field needs to be sampled classically before constructing quantum circuits and the cost of the sampling scales linearly with the time length of the evolution and the momentum grid volume. We will use n -particle states in momentum space as the basis of the Hilbert space and write down matrix elements for the three parts of the Hamiltonian. It will turn out that the kinetic term is diagonal and thus can be efficiently simulated. Furthermore, the matrices of the diffusion and splitting Hamiltonians are sparse, indicating that we are very likely able to efficiently simulate them on a quantum computer. After discretizing momenta and encoding all the basis states in the qubit register, we can construct quantum gates for the Hamiltonian. The initial state of the time evolution for jet quenching is given by one or many partons (quarks and gluons) with definite momenta, colors and spins, properly (anti)symmetrized, which can be easily constructed in the qubit register since it is a linear combination of the basis states with known coefficients. The standard Trotterization method will then be applied to simulate the Hamiltonian evolution. At the end of the time evolution, we perform measurements by projecting the final state onto a state with certain number of partons with specific momenta, colors and spins,

that is properly (anti)symmetrized. Radiation spectra can then be estimated from the measurement results by repeating the time evolution and the projective measurement multiple times. Our approach automatically keeps track of quantum interference, since it is based on the quantum evolution of a wavefunction, i.e., it evolves on the amplitude level. Therefore, our framework can be easily used to study the LPM effect for more than two splittings, no matter whether the medium is time independent or time dependent, thin or thick, hot or cold. In the future, with fault-tolerant quantum computers that have a few hundred logical qubits, we will be able to use this framework to study QCD jet quenching in nuclear environments and learn new physical insights into the LPM effect.

We will apply the formalism to study a toy model that can be encoded by five qubits. The toy model consists of scalar particles, which means we neglect the spin and color degrees of freedom that are present in QCD. To reduce the size of the Hilbert space, we simply consider a $2 + 1$ dimensional system with only one transverse direction. Both the longitudinal and transverse momenta have two levels. We include both 1-particle and 2-particle states in the Hilbert space, which allows us to study the LPM effect in one splitting. Classical background fields are also used to describe the random transverse momentum exchanges in the toy model, which are sampled classically. By explicitly constructing a quantum circuit for the time evolution of the toy model and running simulations on the IBM Qiskit simulator, we compare the total radiation probabilities in vacuum and in the medium for an initial 1-particle state. We find that the probability of having two particles in the final state is smaller in the medium, which means the LPM effect that suppresses radiation is observed in the quantum simulation results of the toy model.

This paper is organized as follows: in Sect. 2 we will give an overview of the framework, which includes state initialization, Hamiltonian time evolution and final measurements. We will introduce the light-front Hamiltonian of QCD to describe the in-medium dynamics of high energy partons and explain the n -particle basis of the Hilbert space. The matrix elements of the three parts of the Hamiltonian: the kinetic, diffusion and splitting terms will be given explicitly in the following Sect. 3, together with a discussion on the sampling of the classical background field. Furthermore, quantum simulation of the toy model for studying the LPM effect will be discussed in Sect. 4, with an explicit construction of the quantum circuit for the time evolution. Simulation results that are based on the IBM Qiskit quantum simulator will also be shown. Finally, we will conclude and give an outlook in Sect. 5.

2 Formalism

A typical diagram to understand the LPM effect in jet quenching is depicted in Fig. 1, which describes the time evolution of a quantum state initiated by an incoming parton that undergoes subsequent soft momentum exchanges, splittings and recombination. The diagram is on the amplitude level. To calculate physical observables, one needs to sum over the amplitudes from all diagrams with the same final state. In general, the number of diagrams grow exponentially with the number of splittings and their quantum interference is extremely difficult to account for in an approach based on perturbative theory.

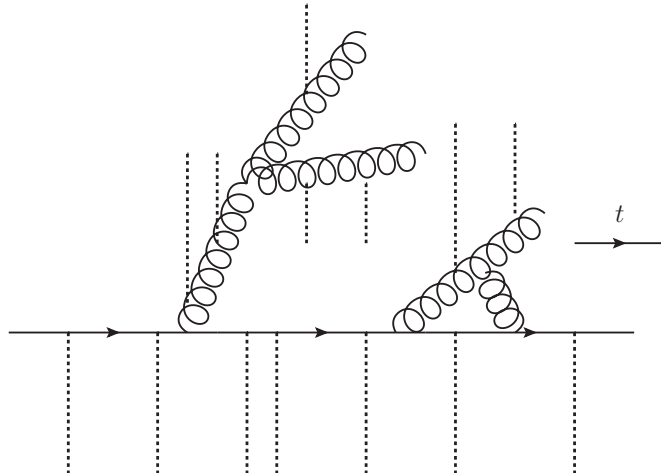


Figure 1: Typical diagram describing the LPM effect in jet quenching on the amplitude level, which includes free propagation, soft momentum exchange (labeled by dashed lines) and splitting/recombination. The solid lines with arrows indicate the propagation of quarks in time, while the curly lines are for the propagation of gluons.

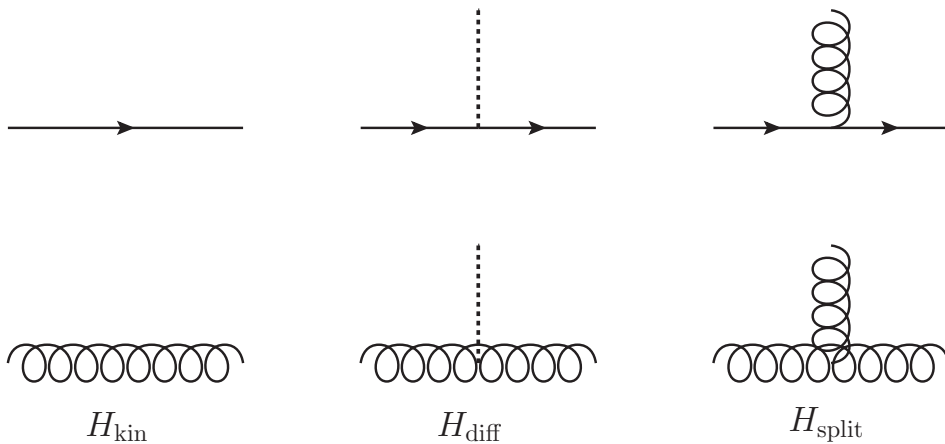


Figure 2: Three parts of the Hamiltonian for studying the LPM effect in jet quenching: the kinetic, diffusion and splitting/recombination terms. Matrix elements of these Hamiltonians will be explicitly given in Section 3.

To simulate the time evolution of jets and study the LPM effect on a quantum computer, we need a Hamiltonian description of the evolution, which includes the kinetic term, diffusion caused by soft momentum transfer from the medium and splitting/recombination, as depicted in Fig. 2. In this work, we will use the light-front Hamiltonian of QCD to describe the dynamics of high energy partons and their interactions with the nuclear medium. A brief introduction to the light-front Hamiltonian of QCD can be found in Appendix A. We will first discuss the light-front Hamiltonian dynamics for studying the LPM effect in jet quenching in Section 2.1. Then in Section 2.2 we will introduce the computational basis

of the Hilbert space for the quantum simulation.

2.1 Light-Front Hamiltonian Dynamics

The light-front Hamiltonian dynamics is determined by

$$2i\frac{\partial}{\partial x^+}|\Psi\rangle = H|\Psi\rangle, \quad (2.1)$$

where $x^+ = x^0 + x^3$ is the light-cone time.¹ Our convention of the light-cone coordinates and the construction of the light-front Hamiltonian of QCD can be found in Appendix A. The light-front Hamiltonian of QCD can be written as

$$H = \int dx^- d^2x_\perp \left(i\psi_+^\dagger (-\not{D}_\perp + im) \frac{1}{\partial^+} (\not{D}_\perp + im)\psi_+ - g\psi_+^\dagger A^{-a} T^a \psi_+ \right. \\ \left. + \frac{1}{4} F_\perp^{ija} F_{\perp ij}^a - \frac{1}{8} (\partial^+ A^{-a})^2 + \frac{1}{2} (\partial^+ A_\perp^{ia}) (-\partial_i A^{-a} + g f^{abc} A^{-b} A_{\perp i}^c) \right), \quad (2.6)$$

where $i = 1, 2$ and $j = 1, 2$ denote the transverse components and are implicitly summed over. The $-$ component of the gauge field is not dynamical and is related to the dynamical components via

$$A^{-a} = \frac{2}{\partial^+} \partial^i A_\perp^{ia} - \frac{2g}{\partial^{+2}} \left(f^{abc} (\partial^+ A_\perp^{ib}) A_\perp^{ic} - 2\psi_+^\dagger T^a \psi_+ \right), \quad (2.7)$$

where $\partial^{+2} = (\partial^+)^2$. The light-front Hamiltonian (2.6) is time independent. The dynamical fields ψ_+^i and A_\perp^{ia} at zero time $x^+ = 0$ can be expanded in terms of creation and annihilation

¹The factor of 2 on the left-hand side is just a convention. When defining the light-front Hamiltonian, we integrate the Hamiltonian density with the integral measure

$$\int dx^- d^2x_\perp \mathcal{H}. \quad (2.2)$$

On the other hand, we know the Lorentz invariant measure in spacetime is

$$\int d^4x = \frac{1}{2} \int dx^+ dx^- d^2x_\perp. \quad (2.3)$$

Therefore, for consistency we need to treat $\frac{1}{2}x^+$ as the “time” conjugated to the Hamiltonian.

Another way of seeing this factor of 2 is to note that $\frac{\partial}{\partial x^+}$ is associated with P_+ and defining P_+ involves

$$\int \varepsilon_{+12-} dx^- dx^1 dx^2, \quad (2.4)$$

where the Levi-Civita tensor is normalized by

$$\varepsilon_{+12-} = \frac{1}{2}, \quad (2.5)$$

when one uses the convention $x^+ = x^0 + x^3$. See e.g., Ref. [137].

operators in momentum space

$$\psi_{\perp}^i(x^+ = 0, x_{\perp}, x^-) = \sum_{\sigma=\pm\frac{1}{2}} \int_{k^+>0} \frac{dk^+ d^2k_{\perp}}{2(2\pi)^3 k^+} \left(b^i(k, \sigma) u_+(k, \sigma) e^{-ik \cdot x} + d^{i\dagger}(k, \sigma) v_+(k, \sigma) e^{ik \cdot x} \right), \quad (2.8)$$

$$A_{\perp}^{ib}(x^+ = 0, x_{\perp}, x^-) = \sum_{\lambda=\pm} \int_{k^+>0} \frac{dk^+ d^2k_{\perp}}{2(2\pi)^3 k^+} \left(a^b(k, \lambda) \varepsilon_{\perp}^i(\lambda) e^{-ik \cdot x} + a^{b\dagger}(k, \lambda) \varepsilon_{\perp}^{i*}(\lambda) e^{ik \cdot x} \right), \quad (2.9)$$

where a, b, d ($a^{\dagger}, b^{\dagger}, d^{\dagger}$) are annihilation (creation) operators for gluons, quarks and anti-quarks respectively. Here σ denotes quark spins, λ represents gluon polarizations and $\varepsilon_{\perp}(\lambda)$ is the corresponding polarization tensor in the transverse plane. The Hamiltonian can be quantized by imposing the following (anti-)commutation relations:

$$\begin{aligned} \{b^i(k, \sigma), b^{j\dagger}(k', \sigma')\} &= \{d^i(k, \sigma), d^{j\dagger}(k', \sigma')\} = 2(2\pi)^3 k^+ \delta^{ij} \delta_{\sigma\sigma'} \delta^3(k - k'), \\ [a^b(k, \lambda), a^{c\dagger}(k', \lambda')] &= 2(2\pi)^3 k^+ \delta_{\lambda\lambda'} \delta^{bc} \delta^3(k - k'), \end{aligned} \quad (2.10)$$

where $\delta^3(k - k') = \delta(k^+ - k'^+) \delta^2(k_{\perp} - k'_{\perp})$.

In the following, when we describe the soft momentum exchange between the QGP and high energy partons, which results in diffusion of the partons in the transverse plane, we will use a description based on a background gauge field \bar{A}^{-a} [88]. The \bar{A}^{-a} field is classical and will be discussed in detail in Section 3.2. To incorporate the classical background field into the Hamiltonian, we simply apply the replacement

$$A^{-a} \rightarrow A^{-a} + \bar{A}^{-a}, \quad (2.11)$$

of which the right hand side is the new $-$ component of the gauge field appearing in the Hamiltonian, with A^{-a} given by Eq. (2.7) and \bar{A}^{-a} the classical background field. In general, the classical background field depends on the light-cone time x^+ , so under the replacement (2.11) the light-front Hamiltonian becomes time dependent through \bar{A}^{-a}

$$H \rightarrow H(x^+) = H[\bar{A}^{-a}(x^+)]. \quad (2.12)$$

The Hamiltonian can be split into three parts for studying the LPM effect in jet quenching:

$$H(x^+) = H_{\text{kin}} + H_{\text{diff}}(x^+) + H_{\text{split}}. \quad (2.13)$$

Here H_{kin} describes the free theory of quarks and gluons on the light front and induces a phase change for each parton in the time evolution. H_{diff} represents the interaction between the QGP medium and quarks/gluons in the system, which originates from Glauber exchanges induced by the background fields and results in the transverse momentum broadening of partons. H_{split} gives the interaction between quarks and gluons, describing the splitting process of n high energy partons going into $n + 1$ partons and the inverse process,

i.e., recombination of partons. It is necessary to include recombination of partons in H_{split} for it to be Hermitian and for the time evolution to be unitary.

To simulate the in-medium jet evolution on a digital quantum computer from $x^+ = 0$ to a time $x^+ \equiv 2t$,² we decompose the total time length into N_t small pieces with a step size $\Delta t = t/N_t$ and apply the standard Trotterization method:

$$\left(e^{-i(H_{\text{kin}}+H_{\text{diff}}+H_{\text{split}})\Delta t} \right)^{N_t} |\Psi\rangle = \left(\prod_j e^{-iH_j\Delta t} e^{\mathcal{O}((\Delta t)^2)} \right)^{N_t} |\Psi\rangle, \quad (2.14)$$

where each H_j is chosen such that we know how to construct the quantum circuit for it and $\sum_j H_j = H_{\text{kin}} + H_{\text{diff}} + H_{\text{split}}$. The error $\mathcal{O}((\Delta t)^2)$ on the right hand side comes from nonzero commutators $[H_j, H_k] \neq 0$ ($j \neq k$). When N_t is large, the correction term $\mathcal{O}((\Delta t)^2)$ can be neglected. Then simulating the in-medium jet evolution can be realized by constructing quantum gates implementing the Hamiltonian dynamics determined by each H_j . The convergence rate of the Trotterization can be further improved by including higher-order corrections.

To write out matrix elements for each part of the Hamiltonian, we need to choose a basis of the Hilbert space to project the Hamiltonian. In the next subsection, we will explain the basis constructed from n -particle states in momentum space.

2.2 Hilbert Space

To formulate the Hamiltonian dynamics on a digital quantum computer, we need to first construct a basis of the physical Hilbert space and discretize it so that we can encode quantum states in terms of qubits and represent the Hamiltonian as quantum gates. We use n -particle states in the light-front momentum space to construct the basis of the Hilbert space. A 1-particle state can be labeled as

$$|q/g, k^+ > 0, k_x, k_y, \text{color}, \text{spin}\rangle : \frac{b^{i\dagger}(k, \sigma)|0\rangle}{\sqrt{2(2\pi)^3 k^+}}, \frac{d^{i\dagger}(k, \sigma)|0\rangle}{\sqrt{2(2\pi)^3 k^+}}, \frac{a^{b\dagger}(k, \lambda)|0\rangle}{\sqrt{2(2\pi)^3 k^+}}, \quad (2.15)$$

which is obtained by applying a creation operator ($a^{b\dagger}$, $b^{i\dagger}$ or $d^{i\dagger}$) on the vacuum. The normalization factor $1/\sqrt{2(2\pi)^3 k^+}$ is chosen for later convenience. Here q/g indicates whether the state is a quark or a gluon. There is no ghost state since in the light-front Hamiltonian formulation of QCD, the light-cone gauge $A^+ = 0$ is chosen and ghosts are decoupled from gluons. The momentum of the state is specified by the $+$ and transverse components: (k^+, k_x, k_y) . In the light-front approach, the $+$ component is always positive so we have constrained the Hilbert space to only contain states with positive k^+ . A quark or an antiquark state has three degrees of freedom in color. We will label both states as q , i.e., a quark state and then differentiate them by the color degrees of freedom. In other words, a quark state has six degrees of freedom in color in our notation, which requires three qubits to encode. A gluon state has eight degrees of freedom in color, which also requires three qubits to encode. The spin degree of freedom has two possibilities for both

²Here t is just a short hand notation for $x^+/2$ and should be distinguished from x^0 used in the definition of $x^+ = x^0 + x^3$.

quark and gluon states, which needs one qubit to store. (For gluon states, by spin we mean the polarization.)

A general n -particle basis state can be written as

$$\bigotimes_{i=1}^n |q/g, k^+ > 0, k_x, k_y, \text{color}, \text{spin}\rangle_i \quad (2.16)$$

where the i -th and j -th states ($i \neq j$) generally differ in momenta and/or quantum numbers. A single n -particle basis state cannot be physical, since physical states of multiple particles need to be properly (anti)symmetrized. For studying the LPM effect, if we start with a 1-particle state, the Hamiltonian evolution will guarantee the final state is properly (anti)symmetrized, since the (anti)symmetric properties of the boson (fermion) creation and annihilation operators are already included in the construction of the Hamiltonian. To simulate the time evolution of a more general initial state for jet quenching, the initial state needs proper (anti)symmetrization. Then the Hamiltonian evolution will lead to a properly (anti)symmetrized final state.

The basis of the Hilbert space consists of n -particle states for all integers n . To simulate the LPM effect in processes with N particles in total (which can happen in cases with one initial parton having $N - 1$ splittings or two initial partons having $N - 2$ splittings, etc), we need to include all the 1-particle states, 2-particle states and all the way to N -particle states in the basis, in order to describe the system. In principle, states with more than N particles can also affect the time evolution through loop effects, i.e., they only exist as intermediate states and are absent in the final states measured. To reduce the loop effects, one may truncate the states with a much high particle number such as $2N$.

Before moving on to the detailed discussion of the Hamiltonian, we give an estimate of the qubit cost. For each 1-particle state, to distinguish a quark state from a gluon one, two degrees of freedom are required. We also need eight color degrees of freedom (a quark state only has six degrees of freedom in color but the more demanding case in terms of the register resource is given by a gluon state) and two spin degrees of freedom. To encode the basis states on a digital quantum computer, we need to truncate and discretize the momenta. We assume the ranges of the momenta are given by

$$k^+ \in (0, K_{\max}^+], \quad k_x \in [-K_{\max}^\perp, K_{\max}^\perp], \quad k_y \in [-K_{\max}^\perp, K_{\max}^\perp]. \quad (2.17)$$

With step sizes set by $\Delta k^+, \Delta k^\perp, \Delta k^\perp$ for the $+, x, y$ components respectively, the number of degrees of freedom in momenta is given by $N^+ N_\perp^2$ where

$$N^+ = \frac{K_{\max}^+}{\Delta k^+}, \quad N_\perp = \frac{K_{\max}^\perp}{\Delta k^\perp} + 1. \quad (2.18)$$

Therefore, the number of qubits needed to represent all the 1-particle states is estimated as

$$\log_2(2^5 N^+ N_\perp^2). \quad (2.19)$$

Encoding all the n -particle states (fixed n) requires a number of qubits given by

$$\log_2 \left((2^5 N^+ N_\perp^2)^n \right). \quad (2.20)$$

If we want to study the LPM effect in processes with N particles in total with loop effects from states of more than N particles neglected, we have to include all the n -particle states where $n = 1, 2, \dots, N$. The total number of qubits needed in the register then is

$$\log_2 \left(\sum_{n=1}^N (2^5 N^+ N_{\perp}^2)^n \right). \quad (2.21)$$

One can reduce the qubit cost in the register for special cases. For example, if we study the LPM effect in a process initiated by one parton, the qubit cost is given by

$$\log_2 \left(\sum_{n=1}^N \frac{1}{n!} (2^5 N^+ N_{\perp}^2)^n \right), \quad (2.22)$$

where the $1/n!$ factor originates from the constraint that $k^+ > 0$ and the total $+$ component of the momentum is conserved in each splitting. In general, the qubit cost is estimated by Eq. (2.21). If we choose $N^+ = N_{\perp} = 100$, the cost of qubit numbers is about 50 for one initial parton having one splitting and about 75 for two splittings, according to Eq. (2.21). To go beyond the scope of current studies of the LPM effect, we will simulate the case with one initial parton and three splittings, which needs about 100 qubits. In the NISQ era, a quantum simulation using 100 qubits is possible, but error mitigation techniques are necessary for physical applications. Fault-tolerant quantum computers with 100 qubits may become available in the near future.

2.3 State Initialization and Measurement

For studies of the LPM effect, the initial state contains a number of partons with specific momenta, colors and spins and each of them can be either a quark or a gluon. Therefore the initial state is just a linear combination of n -particle basis states, properly (anti)symmetrized, and it can be easily initialized in the qubit register. The initialization is much simpler than cases where the initial states involve hadrons such as protons, which are nontrivial linear superposition of all n -particle states, with coefficients that are a priori unknown. Adiabatic state preparation has been proposed to prepare such complicated initial states by starting with free particles and then slowly turning on the interaction [138]. Here we only focus on quantum simulation of the LPM effect in medium-induced radiation for one or a number of initial partons. Quantum simulation of the whole heavy ion collision where the initial state consists of two heavy nuclei, which are complicated nuclear bound states, is beyond the scope of our current study.

The final state contains multi-particle states due to the splittings in the time evolution. To extract the radiation spectrum from the final state, we project the final state onto a specific n -particle state with given momenta, colors and spins, which corresponds to a specific state in the computational basis or a linear combination of the basis states with known coefficients. So the measurement is simply projective. The time evolution and the projective measurement need repeating multiple times since the quantum state collapses after the measurement. After collecting enough statistics, one will be able to calculate the radiation spectrum. Color and spin degrees of freedom may be averaged, depending on the radiation spectrum of interest.

3 Matrix Elements of the Light-Front Hamiltonian of QCD

In this section, we will write down matrix elements of the light-front Hamiltonian of QCD in the computational basis introduced in the previous section, for the kinetic H_{kin} , diffusion H_{diff} and splitting H_{split} terms.

3.1 Kinetic Term

The kinetic energy parts of the Hamiltonian are given by

$$H_{f, \text{kin}} = \sum_i \sum_{\sigma=\pm\frac{1}{2}} \int_{k^+>0} \frac{dk^+ d^2k_\perp \mathbf{k}_\perp^2}{2(2\pi)^3 k^+ k^+} \left(b^{i\dagger}(k, \sigma) b^i(k, \sigma) + d^{i\dagger}(k, \sigma) d^i(k, \sigma) \right), \quad (3.1)$$

$$H_{g, \text{kin}} = \sum_b \sum_{\lambda=\pm} \int_{k^+>0} \frac{dk^+ d^2k_\perp \mathbf{k}_\perp^2}{2(2\pi)^3 k^+ k^+} a^{b\dagger}(k, \lambda) a^b(k, \lambda),$$

for quarks and gluons respectively. The derivation of these terms can be found in Appendix A. Matrix elements of the kinetic terms in the basis of Eq. (2.15) are given by

$$\langle q, k_1^+, k_{1\perp}, i_1, \sigma_1 | H_{q, \text{kin}} | q, k_2^+, k_{2\perp}, i_2, \sigma_2 \rangle = \frac{\mathbf{k}_{1\perp}^2}{k_1^+} \delta(k_1^+ - k_2^+) \delta^2(k_{1\perp} - k_{2\perp}) \delta_{i_1 i_2} \delta_{\sigma_1 \sigma_2}, \quad (3.2)$$

$$\langle g, k_1^+, k_{1\perp}, a_1, \lambda_1 | H_{g, \text{kin}} | g, k_2^+, k_{2\perp}, a_2, \lambda_2 \rangle = \frac{\mathbf{k}_{1\perp}^2}{k_1^+} \delta(k_1^+ - k_2^+) \delta^2(k_{1\perp} - k_{2\perp}) \delta_{a_1 a_2} \delta_{\lambda_1 \lambda_2},$$

which in the discretized computational basis becomes

$$\langle q, k_1^+, k_{1\perp}, i_1, \sigma_1 | H_{q, \text{kin}} | q, k_2^+, k_{2\perp}, i_2, \sigma_2 \rangle = \frac{\mathbf{k}_{1\perp}^2}{k_1^+} \delta_{k_1^+ k_2^+} \delta_{k_{1x} k_{2x}} \delta_{k_{1y} k_{2y}} \delta_{i_1 i_2} \delta_{\sigma_1 \sigma_2}, \quad (3.3)$$

$$\langle g, k_1^+, k_{1\perp}, a_1, \lambda_1 | H_{g, \text{kin}} | g, k_2^+, k_{2\perp}, a_2, \lambda_2 \rangle = \frac{\mathbf{k}_{1\perp}^2}{k_1^+} \delta_{k_1^+ k_2^+} \delta_{k_{1x} k_{2x}} \delta_{k_{1y} k_{2y}} \delta_{a_1 a_2} \delta_{\lambda_1 \lambda_2}.$$

These matrix elements can be easily generalized to the case with n -particle states that are symbolically represented as $\bigotimes_{i=1}^n |i\rangle \equiv |123 \cdots n\rangle$ where $|i\rangle$ labels the i -th particle state $|q/g, k^+, k_\perp, \text{color}, \text{spin}\rangle_i$:

$$\begin{aligned} & \langle 1'2'3' \cdots n' | H_{\text{kin}} | 123 \cdots n \rangle \\ &= \sum_{i=1}^n \langle i' | H_{\text{kin}} | i \rangle \langle 1'2'3' \cdots (i'-1)(i'+1) \cdots n' | 123 \cdots (i-1)(i+1) \cdots n \rangle \\ &= \sum_{i=1}^n \frac{\mathbf{k}_{i\perp}^2}{k_i^+} \delta_{1'1} \delta_{2'2} \cdots \delta_{n'n}, \end{aligned} \quad (3.4)$$

where $\langle i' | H_{\text{kin}} | i \rangle$ is given by Eq. (3.3) and $\delta_{i'i}$ is a short hand notation for the Kronecher delta functions of the discrete momenta, colors and spins for parton i' and parton i . No cross terms of the form $\langle i' | H_{\text{kin}} | j \rangle$ ($i \neq j$) appear in the matrix elements involving two n -particle states. We want to emphasize this is just a result of our choice of the computational

basis. Such cross terms $\langle i' | H_{\text{kin}} | j \rangle$ ($i \neq j$) are physical and can be accounted for when the quantum state is properly (anti)symmetrized, i.e., such cross terms will show up in the matrix elements of H_{kin} involving two physical states.

With our choice of the computational basis, the kinetic term H_{kin} is diagonal and the diagonal element is given by the light-cone energy of the corresponding n -particle state:

$$\sum_{i=1}^n \frac{\mathbf{k}_{i\perp}^2}{k_i^+}, \quad (3.5)$$

where the summation is over all the constituents in the n -particle state. The time evolution induced by the kinetic Hamiltonian is just a phase, which can be efficiently simulated on a quantum computer by using, e.g., the phase kickback method, which is briefly reviewed in Appendix B. We will also give an explicit construction of the quantum circuit for the kinetic evolution in Section 4, which does not rely on the phase kickback method.

3.2 Diffusion Term

To describe the diffusion process in the transverse plane caused by the soft momentum transfer from the medium, we replace the A^{-a} field in Eq. (2.6) with $A^{-a} + \bar{A}^{-a}$ where A^{-a} is determined by the dynamical field degrees of freedom as shown in Eq. (2.7) and \bar{A}^{-a} denotes a classical background field. We follow Ref. [88] to describe the medium as a source of the background gauge field \bar{A}^{-a} , which can be time dependent. We assume the background field is x^- independent

$$\bar{A}^{-a}(x^+, x^-, x_\perp) = \bar{A}^{-a}(x^+, x^- = 0, x_\perp), \quad (3.6)$$

since a high energy parton has a large $+$ component of momentum k^+ , thus only probing the medium at a small $x^- \sim 1/k^+$. From now on, we will omit the dependence of the background gauge field on the x^- coordinate.

We further assume the random background field satisfies the two-point correlation

$$\langle \bar{A}^{-a}(x^+, x_\perp) \bar{A}^{-b}(y^+, y_\perp) \rangle = \delta^{ab} \delta(x^+ - y^+) \gamma(\mathbf{x}_\perp - \mathbf{y}_\perp). \quad (3.7)$$

The random background fields at different light-cone times are assumed independent. One can replace the $\delta(x^+ - y^+)$ function with some other functions in $x^+ - y^+$ to describe some correlation between the random background fields at different times. The $\gamma(\mathbf{x}_\perp - \mathbf{y}_\perp)$ function accounts for nontrivial correlation between background fields at the same light-cone time but different transverse positions. The model used in Ref. [88] is motivated from the hard-thermal-loop calculation of the Landau damping phenomenon

$$\gamma(\mathbf{x}_\perp - \mathbf{y}_\perp) = g^2 \int \frac{d^2 q_\perp}{(2\pi)^2} e^{i\mathbf{q}_\perp \cdot (\mathbf{x}_\perp - \mathbf{y}_\perp)} \frac{\pi T m_D^2}{(\mathbf{q}_\perp^2 + m_D^2)^2}, \quad (3.8)$$

where T denotes the temperature of the plasma and m_D is the Debye mass. Our framework of the quantum simulation for jet quenching is general and the construction does not depend on any specific form of the correlation function. In momentum space, the correlation function of the background gauge field is given by

$$\langle \bar{A}^{-a}(k^-, k_\perp) \bar{A}^{-b}(-k^-, -k_\perp) \rangle = \delta^{ab} \gamma(\mathbf{k}_\perp). \quad (3.9)$$

It turns out to be easier to use the mixed space representation

$$\langle \bar{A}^{-a}(x^+, k_\perp) \bar{A}^{-b}(y^+, -k_\perp) \rangle = \delta^{ab} \delta(x^+ - y^+) \gamma(\mathbf{k}_\perp). \quad (3.10)$$

The quark diffusion term in the Hamiltonian can be obtained from terms of the form $\psi_+^\dagger \bar{A}^- \psi_+$. Since the background field \bar{A}^{-a} is x^- independent, we find

$$\partial^+ \bar{A}^{-a}(x^+, x_\perp) = \frac{\partial}{\partial x_+} \bar{A}^{-a}(x^+, x_\perp) = 2 \frac{\partial}{\partial x^-} \bar{A}^{-a}(x^+, x_\perp) = 0. \quad (3.11)$$

Therefore the term $(\partial^+ A^{-a} + \partial^+ \bar{A}^{-a})^2$ in the Hamiltonian (2.6) is irrelevant to the quark diffusion process, which is not obvious from the beginning, since A^{-a} contains $\psi_+^\dagger T^a \psi_+$. With this simplification, the quark diffusion Hamiltonian can be written as

$$\begin{aligned} H_{q, \text{diff}} &= -g \int dx^- d^2 x_\perp \psi_+^\dagger(x) \bar{A}^{-a}(x) T^a \psi_+(x) \\ &= -g \int dx^- d^2 x_\perp \sum_{\sigma_1, \sigma_2} \int_{k_1^+ > 0} \frac{dk_1^+ d^2 k_{1\perp}}{2(2\pi)^3 k_1^+} \int_{k_2^+ > 0} \frac{dk_2^+ d^2 k_{2\perp}}{2(2\pi)^3 k_2^+} \\ &\quad \left(b^{i\dagger}(k_1, \sigma_1) u_+^\dagger(k_1, \sigma_1) e^{ik_1 \cdot x} + d^i(k_1, \sigma_1) v_+^\dagger(k_1, \sigma_1) e^{-ik_1 \cdot x} \right) \bar{A}^{-a}(x) T_{ij}^a \\ &\quad \left(b^j(k_2, \sigma_2) u_+(k_2, \sigma_2) e^{-ik_2 \cdot x} + d^{j\dagger}(k_2, \sigma_2) v_+(k_2, \sigma_2) e^{ik_2 \cdot x} \right). \end{aligned} \quad (3.12)$$

Since $\bar{A}^a(x)$ is x^- independent, the integration over x^- can be carried out to give a delta function in the $+$ component of the momenta:

$$\int dx^- e^{i(k_1^+ x^- \pm k_2^+ x^-)/2} = 2(2\pi) \delta(k_1^+ \pm k_2^+). \quad (3.13)$$

Since both $k_1^+ > 0$ and $k_2^+ > 0$, the delta function with the plus sign vanishes. Then we have

$$\begin{aligned} H_{q, \text{diff}} &= -g \sum_{\sigma_1, \sigma_2} \int_{k_1^+ > 0} \frac{dk_1^+}{2(2\pi)(k_1^+)^2} \int \frac{d^2 k_{1\perp}}{(2\pi)^2} \int \frac{d^2 k_{2\perp}}{(2\pi)^2} \\ &\quad \left(b^{i\dagger}(k_1, \sigma_1) T_{ij}^a b^j(k_2, \sigma_2) u_+^\dagger(k_1, \sigma_1) u_+(k_2, \sigma_2) \bar{A}^{-a}(x^+, \mathbf{k}_{1\perp} - \mathbf{k}_{2\perp}) \right. \\ &\quad \left. + d^i(k_1, \sigma_1) T_{ij}^a d^{j\dagger}(k_2, \sigma_2) v_+^\dagger(k_1, \sigma_1) v_+(k_2, \sigma_2) \bar{A}^{-a}(x^+, -\mathbf{k}_{1\perp} + \mathbf{k}_{2\perp}) \right) \Big|_{k_2^+ = k_1^+}. \end{aligned} \quad (3.14)$$

When $k_1^+ \gg k_{1\perp}, k_{2\perp}, m$, we have

$$\begin{aligned} u_+^\dagger(k_1, \sigma_1) u_+(k_2, \sigma_2) \Big|_{k_1^+ = k_2^+} &= k_1^+ \delta_{\sigma_1 \sigma_2} + \mathcal{O}\left(\frac{k_{1\perp}}{k_1^+}, \frac{k_{2\perp}}{k_1^+}, \frac{m}{k_1^+}\right), \\ v_+^\dagger(k_1, \sigma_1) v_+(k_2, \sigma_2) \Big|_{k_1^+ = k_2^+} &= k_1^+ \delta_{\sigma_1 \sigma_2} + \mathcal{O}\left(\frac{k_{1\perp}}{k_1^+}, \frac{k_{2\perp}}{k_1^+}, \frac{m}{k_1^+}\right), \end{aligned} \quad (3.15)$$

which means in the high energy limit, the spin of a quark does not change under a small transverse perturb. Under the high energy approximation, we take the leading terms and

obtain

$$\begin{aligned}
H_{g, \text{diff}} = & \quad (3.16) \\
& -g \sum_{\sigma} \int_{k_1^+ > 0} \frac{dk_1^+}{2(2\pi)k_1^+} \int \frac{d^2k_{1\perp}}{(2\pi)^2} \int \frac{d^2k_{2\perp}}{(2\pi)^2} \left(b^{i\dagger}(k_1, \sigma) T_{ij}^a b^j(k_2, \sigma) \bar{A}^{-a}(x^+, \mathbf{k}_{1\perp} - \mathbf{k}_{2\perp}) \right. \\
& \quad \left. + d^i(k_1, \sigma) T_{ij}^a d^{j\dagger}(k_2, \sigma) \bar{A}^{-a}(x^+, -\mathbf{k}_{1\perp} + \mathbf{k}_{2\perp}) \right) \Big|_{k_2^+ = k_1^+},
\end{aligned}$$

in which up to a constant, we can switch the order of $d^i(k_1, \sigma)$ and $d^{j\dagger}(k_2, \sigma)$ in the second term and obtain a negative sign due to the anticommutation relation.

The gluon diffusion Hamiltonian can be similarly worked out, which involves terms of the form $A_{\perp} \bar{A}^{-a} A_{\perp}$. First, the F_{\perp}^2 term in the Hamiltonian (2.6) does not involve any \bar{A}^{-a} field, so it is irrelevant for the gluon diffusion process. Furthermore the term $(\partial^+ A^{-a} + \partial^+ \bar{A}^{-a})^2$ in Eq. (2.6) is also irrelevant since the background gauge field \bar{A}^{-a} is x^- independent. The remaining part of the gluon Hamiltonian for consideration is

$$\int dx^- d^2x_{\perp} \frac{1}{2} (\partial^+ A_{\perp}^{ia}) (-\partial_i (A^{-a} + \bar{A}^{-a}) + g f^{abc} (A^{-b} + \bar{A}^{-b}) A_{\perp i}^c). \quad (3.17)$$

Integration by parts and using $\partial^+ \bar{A}^{-a} = 0$ lead to the following Hamiltonian describing the gluon diffusion process (we omit terms without any \bar{A}^{-a})

$$\begin{aligned}
H_{g, \text{diff}} = & -\frac{g}{2} f^{abc} \int dx^- d^2x_{\perp} A_{\perp}^{ia}(x) \bar{A}^{-b}(x) \partial^+ A_{\perp i}^c(x) \quad (3.18) \\
= & -\frac{g}{2} f^{abc} \int dx^- d^2x_{\perp} \sum_{\lambda_1, \lambda_2} \int_{k_1^+ > 0} \frac{dk_1^+ d^2k_{1\perp}}{2(2\pi)^3 k_1^+} \int_{k_2^+ > 0} \frac{dk_2^+ d^2k_{2\perp}}{2(2\pi)^3 k_2^+} \\
& \left(a^a(k_1, \lambda_1) \varepsilon_{\perp}^i(\lambda_1) e^{-ik_1 \cdot x} + a^{a\dagger}(k_1, \lambda_1) \varepsilon_{\perp}^{i*}(\lambda_1) e^{ik_1 \cdot x} \right) \bar{A}^{-b}(x) \\
& \left(-ik_2^+ a^c(k_2, \lambda_2) \varepsilon_{\perp i}(\lambda_2) e^{-ik_2 \cdot x} + ik_2^+ a^{c\dagger}(k_2, \lambda_2) \varepsilon_{\perp i}^*(\lambda_2) e^{ik_2 \cdot x} \right).
\end{aligned}$$

Since the background gauge field \bar{A}^{-a} is x^- independent, we can use Eq. (3.13) to show

$$\begin{aligned}
H_{g, \text{diff}} = & -\frac{ig}{2} f^{abc} \sum_{\lambda_1, \lambda_2} \int_{k_1^+ > 0} \frac{dk_1^+}{2(2\pi)k_1^+} \int \frac{d^2k_{1\perp}}{(2\pi)^2} \int \frac{d^2k_{2\perp}}{(2\pi)^2} \quad (3.19) \\
& \left(a^a(k_1, \lambda_1) \varepsilon_{\perp}^i(\lambda_1) a^{c\dagger}(k_2, \lambda_2) \varepsilon_{\perp i}^*(\lambda_2) \bar{A}^{-b}(x^+, -\mathbf{k}_{1\perp} + \mathbf{k}_{2\perp}) \right. \\
& \quad \left. - a^{a\dagger}(k_1, \lambda_1) \varepsilon_{\perp}^{i*}(\lambda_1) a^c(k_2, \lambda_2) \varepsilon_{\perp i}(\lambda_2) \bar{A}^{-b}(x^+, \mathbf{k}_{1\perp} - \mathbf{k}_{2\perp}) \right) \Big|_{k_1^+ = k_2^+}.
\end{aligned}$$

In the high energy limit $k_1^+ \gg k_{1\perp}, k_{2\perp}, m$, the polarizations λ_1 and λ_2 are defined with respect to the same axis along which k_1^+ is aligned. So we have the simplification

$$\sum_{i=1,2} \varepsilon_{\perp}^i(\lambda_1) \varepsilon_{\perp i}^*(\lambda_2) = -\delta_{\lambda_1 \lambda_2}. \quad (3.20)$$

Then we have

$$\begin{aligned}
H_{g, \text{diff}} & \tag{3.21} \\
&= \frac{ig}{2} f^{abc} \sum_{\lambda} \int_{k_1^+ > 0} \frac{dk_1^+}{2(2\pi)k_1^+} \int \frac{d^2k_{1\perp}}{(2\pi)^2} \int \frac{d^2k_{2\perp}}{(2\pi)^2} \left(a^a(k_1, \lambda) a^{c\dagger}(k_2, \lambda) \bar{A}^{-b}(x^+, -\mathbf{k}_{1\perp} + \mathbf{k}_{2\perp}) \right. \\
& \quad \left. - a^{a\dagger}(k_1, \lambda) a^c(k_2, \lambda) \bar{A}^{-b}(x^+, \mathbf{k}_{1\perp} - \mathbf{k}_{2\perp}) \right) \Big|_{k_1^+ = k_2^+}.
\end{aligned}$$

Up to a constant in $H_{g, \text{diff}}$, we are allowed to switch the order of $a^a(k_1, \lambda)$ and $a^{c\dagger}(k_2, \lambda)$ in the first term of $H_{g, \text{diff}}$.

With Eqs. (3.16) and (3.21) describing the transverse diffusion processes for quarks and gluons, we can write out the matrix elements of the diffusion Hamiltonian

$$\begin{aligned}
& \langle q, k_1^+, k_{1\perp}, i_1, \sigma_1 | H_{q, \text{diff}}(x^+) | q, k_2^+, k_{2\perp}, i_2, \sigma_2 \rangle \tag{3.22} \\
&= \begin{cases} -\frac{g}{(2\pi)^2} \delta(k_1^+ - k_2^+) \delta_{\sigma_1 \sigma_2} T_{i_1 i_2}^a \bar{A}^{-a}(x^+, \mathbf{k}_{1\perp} - \mathbf{k}_{2\perp}) & \text{for quark} \\ +\frac{g}{(2\pi)^2} \delta(k_1^+ - k_2^+) \delta_{\sigma_1 \sigma_2} T_{i_2 i_1}^a \bar{A}^{-a}(x^+, \mathbf{k}_{1\perp} - \mathbf{k}_{2\perp}) & \text{for antiquark} \end{cases}, \\
& \langle g, k_1^+, k_{1\perp}, a_1, \lambda_1 | H_{g, \text{diff}}(x^+) | g, k_2^+, k_{2\perp}, a_2, \lambda_2 \rangle \\
&= \frac{ig}{(2\pi)^2} \delta(k_1^+ - k_2^+) \delta_{\lambda_1 \lambda_2} f^{a_2 b a_1} \bar{A}^{-b}(x^+, \mathbf{k}_{1\perp} - \mathbf{k}_{2\perp}).
\end{aligned}$$

Using $\bar{A}^{-a}(\mathbf{k}_{\perp}) = \bar{A}^{-a}(-\mathbf{k}_{\perp})$, we can also show these matrices are Hermitian. In these matrix elements, nontrivial color rotations occur in addition to the transverse momentum exchange. With discretized momenta, we will replace $\delta(k_1^+ - k_2^+)$ with $\delta_{k_1^+ k_2^+}$.

It is easy to generalize the matrix elements for n -particle states $\bigotimes_{i=1}^n |i\rangle \equiv |123 \cdots n\rangle$ where $|i\rangle$ labels the i -th particle state $|q/g, k^+, k_{\perp}, \text{color, spin}\rangle_i$. Since the diffusion process does not change the number of particles in the state and only changes the transverse momentum and color of the state, a matrix element involving two states with different particle numbers vanishes

$$\langle 1'2'3' \cdots n' | H_{\text{diff}} | 123 \cdots n \rangle = 0, \quad \text{if } n \neq n'. \tag{3.23}$$

When the two states have the same number of particles, we have

$$\begin{aligned}
& \langle 1'2'3' \cdots n' | H_{\text{diff}} | 123 \cdots n \rangle \tag{3.24} \\
&= \sum_{i=1}^n \langle i' | H_{\text{diff}} | i \rangle \langle 1'2'3' \cdots (i'-1)(i'+1) \cdots n' | 123 \cdots (i-1)(i+1) \cdots n \rangle \\
&= \sum_{i=1}^n \langle i' | H_{\text{diff}} | i \rangle \delta_{1'1} \delta_{2'2} \cdots \delta_{(i'-1)(i-1)} \delta_{(i'+1)(i+1)} \cdots \delta_{n'n}.
\end{aligned}$$

Cross terms of the form $\langle i' | H_{\text{diff}} | j \rangle$ ($i \neq j$) are accounted for by properly (anti)symmetrized quantum states, as in the case of the kinetic term discussed above. The matrix elements between two states with different k_i^+ s, spins or polarizations also vanish, no matter whether they have the same number of particles or not. Therefore, the matrix representing the

diffusion Hamiltonian is sparse and thus we expect that encoding it on a quantum computer does not require an exponential number of gates.

The diffusion Hamiltonian that we have constructed is general and valid not only for background fields satisfying Eq. (3.10), but also for other background fields that satisfy certain higher-point correlation functions, which will only affect our sampling method when generating the background fields. Once the classical background fields are sampled at each time step, they can be plugged into the diffusion Hamiltonian constructed above. In Section 3.4, we will discuss how to sample the background fields according to Eq. (3.10).

3.3 Splitting Term

Finally we work out the matrix elements of the Hamiltonian describing the parton splitting process and its inverse. The full Hamiltonian (2.6) contains both $1 \rightarrow 2$ and $1 \rightarrow 3$ splittings, as well as $2 \rightarrow 1$, $2 \rightarrow 2$ and $3 \rightarrow 1$ processes. For simplicity, we will focus on the $1 \rightarrow 2$ splitting and its inverse process in this paper. The Hamiltonian for the other processes is either one order higher in the coupling strength g or at least one order higher in the inverse of the large longitudinal momentum $\frac{1}{\partial^+}$ than the $1 \rightarrow 2$ splitting. Therefore, these $1 \rightarrow 3$, $2 \rightarrow 2$ and $3 \rightarrow 1$ processes are suppressed in the high energy limit, either by the coupling strength or by the large longitudinal momentum $1/k^+$. For completeness, all the operators in the Hamiltonian (2.6) describing splitting processes are listed in Appendix A.3, organized by powers of g and $\frac{1}{\partial^+}$.

The $1 \rightarrow 2$ splitting and its inverse process that involve quarks happen at the order $\mathcal{O}(\frac{g}{\partial^+})$. The relevant Hamiltonian is

$$H_{q, \text{split}} = -g \int dx^- dx_{\perp}^2 \left[\psi_+^\dagger A_{\perp i} \gamma^i \gamma^j \left(\frac{\partial_{\perp j}}{\partial^+} \psi_+ \right) + \left(\frac{\partial_{\perp i}}{\partial^+} \psi_+^\dagger \right) A_{\perp j} \gamma^i \gamma^j \psi_+ + 2\psi_+^\dagger T^a \psi_+ \left(\frac{\partial^i}{\partial^+} A_{\perp}^{ia} \right) \right], \quad (3.25)$$

where we have neglected the terms proportional to the quark mass m . The $1 \rightarrow 2$ splitting and its inverse with three gluons involved start to occur at the order $\mathcal{O}(g)$. In other words, the $1 \rightarrow 2$ splitting with quarks involved is suppressed by one power in $\frac{1}{\partial^+}$ with respect to that with only gluons involved and thus suppressed in the high energy limit. Collecting relevant terms shown in Appendix A.3, we find the splitting Hamiltonian with three gluons involved can be written as

$$H_{g, \text{split}} = g f^{abc} \int dx^- dx_{\perp}^2 \left[(\partial^+ A_{\perp}^{ia}) \left(\frac{\partial^j}{\partial^+} A_{\perp}^{jb} \right) A_{\perp i}^c - (\partial^i A_{\perp}^{ja}) A_{\perp i}^b A_{\perp j}^c \right]. \quad (3.26)$$

The matrix elements of the $1 \rightarrow 2$ splitting for a quark or a gluon are given by

$$\begin{aligned}
& \langle q, k_2^+, k_{2\perp}, i_2, \sigma_2; g, q^+, q_\perp, a, \lambda | H_{q, \text{split}} | q, k_1^+, k_{1\perp}, i_1, \sigma_1 \rangle \\
&= -\frac{g}{\sqrt{2(2\pi)^3 q^+ k_1^+ k_2^+}} \delta(k_1^+ - k_2^+ - q^+) \delta^2(k_{1\perp} - k_{2\perp} - q_\perp) \\
&\quad \times \bar{u}(k_2, \sigma_2) \left(\epsilon_\perp^i \gamma^i \gamma^j \frac{k_{1\perp}^j}{k_1^+} T_{i_2 i_1}^a + \frac{k_{2\perp}^i}{k_2^+} \gamma^i \gamma^j \epsilon_\perp^j T_{i_2 i_1}^a + 2T_{i_2 i_1}^a \frac{q_\perp^i}{q^+} \epsilon_\perp^i \right) u(k_1, \sigma_1), \\
& \langle g, -k_2^+, -k_{2\perp}, a_2, \lambda_2; g, -k_3^+, -k_{3\perp}, a_3, \lambda_3 | H_{g, \text{split}} | g, k_1^+, k_{1\perp}, a_1, \lambda_1 \rangle \\
&= -\frac{ig}{\sqrt{2(2\pi)^3 k_1^+ k_2^+ k_3^+}} f^{abc} \delta(k_1^+ + k_2^+ + k_3^+) \delta^2(k_{1\perp} + k_{2\perp} + k_{3\perp}) \\
&\quad \left(k_1^+ \epsilon_\perp^i(\lambda_1) \left[\frac{k_{2\perp}^j}{k_2^+} \epsilon_\perp^j(\lambda_2) \epsilon_{\perp i}(\lambda_3) - \frac{k_{3\perp}^j}{k_3^+} \epsilon_\perp^j(\lambda_3) \epsilon_{\perp i}(\lambda_2) \right] + k_2^+ \epsilon_\perp^i(\lambda_2) \left[\frac{k_{3\perp}^j}{k_3^+} \epsilon_\perp^j(\lambda_3) \epsilon_{\perp i}(\lambda_1) \right. \right. \\
&\quad \left. \left. - \frac{k_{1\perp}^j}{k_1^+} \epsilon_\perp^j(\lambda_1) \epsilon_{\perp i}(\lambda_3) \right] + k_3^+ \epsilon_\perp^i(\lambda_3) \left[\frac{k_{1\perp}^j}{k_1^+} \epsilon_\perp^j(\lambda_1) \epsilon_{\perp i}(\lambda_2) - \frac{k_{2\perp}^j}{k_2^+} \epsilon_\perp^j(\lambda_2) \epsilon_{\perp i}(\lambda_1) \right] \right. \\
&\quad \left. - k_{1\perp}^i \epsilon_\perp^j(\lambda_1) \left[\epsilon_{\perp i}(\lambda_2) \epsilon_{\perp j}(\lambda_3) - \epsilon_{\perp i}(\lambda_3) \epsilon_{\perp j}(\lambda_2) \right] - k_{2\perp}^i \epsilon_\perp^j(\lambda_2) \left[\epsilon_{\perp i}(\lambda_3) \epsilon_{\perp j}(\lambda_1) \right. \right. \\
&\quad \left. \left. - \epsilon_{\perp i}(\lambda_1) \epsilon_{\perp j}(\lambda_3) \right] - k_{3\perp}^i \epsilon_\perp^j(\lambda_3) \left[\epsilon_{\perp i}(\lambda_1) \epsilon_{\perp j}(\lambda_2) - \epsilon_{\perp i}(\lambda_2) \epsilon_{\perp j}(\lambda_1) \right] \right),
\end{aligned} \tag{3.27}$$

where we used negative momenta to label the outgoing states in the splitting involving three gluons, which allows us to easily keep track of the signs. Physical states should have positive $+$ components of the momenta and the matrix elements of the splitting Hamiltonian for physical outgoing states can be easily obtained by flipping the signs of the momenta for the outgoing particles. The matrix elements of the splitting Hamiltonian can be easily generalized for cases with n initial partons, which describe $n \rightarrow n + 1$ splitting processes:

$$\begin{aligned}
& \langle 1'2'3' \dots n'(n'+1) | H_{\text{split}} | 123 \dots n \rangle \\
&= \sum_{i=1}^n \langle i'(n'+1) | H_{\text{split}} | i \rangle \langle 1'2'3' \dots (i'-1)(i'+1) \dots n' | 123 \dots (i-1)(i+1) \dots n \rangle \\
&= \sum_{i=1}^n \langle i'(n'+1) | H_{\text{split}} | i \rangle \delta_{1'1} \delta_{2'2} \dots \delta_{(i'-1)(i-1)} \delta_{(i'+1)(i+1)} \dots \delta_{n'n},
\end{aligned} \tag{3.28}$$

where terms of the form $\langle i'(n'+1) | H_{\text{split}} | j \rangle$ ($i \neq j$) do not contribute. They are properly accounted for by the (anti)symmetric property of a quantum state. As can be seen, the matrix for the splitting Hamiltonian is also sparse.

The matrix representing the splitting Hamiltonian is not Hermitian. Its Hermitian conjugate gives the matrix for the inverse process, which describes parton recombination. It is essential to include parton recombination to reproduce the virtual correction diagrams in the usual Feynman diagram approach to study the LPM effect.

3.4 Sampling Classical Background Field

The diffusion part of the Hamiltonian is light-cone time dependent and the dependence is through the random classical background field \bar{A}^{-a} , which satisfies the correlation (3.10).

To generate the matrix elements of the diffusion Hamiltonian, we need to generate the random classical background fields at each time step in the Trotterization, which can be done by sampling random variables according to the correlation. In the discretized version, the correlation can be written as

$$\langle \bar{A}^{-a}(x^+, k_\perp) \bar{A}^{-b}(y^+, -k_\perp) \rangle = \delta^{ab} \delta_{x^+ y^+} \gamma(\mathbf{k}_\perp), \quad (3.29)$$

where $\delta_{x^+ y^+}$ is a Kronecker delta function for the discretized light-cone time. The delta function in time means the classical background fields at different times are independent, and thus can be sampled independently. At a given time x^+ , the correlation that governs the distribution of the background field is written as

$$\langle \bar{A}^{-a}(x^+, k_\perp) \bar{A}^{-a}(x^+, -k_\perp) \rangle = \gamma(\mathbf{k}_\perp), \quad (3.30)$$

which almost corresponds to the width of a Gaussian distribution for the random variable $\bar{A}^{-a}(x^+, k_\perp)$. The obstacle is in the sign difference between the k_\perp arguments of the two random fields. In other words, $\bar{A}^{-a}(x^+, k_\perp)$ and $\bar{A}^{-a}(x^+, -k_\perp)$ are two different random variables for $k_\perp \neq 0$.

To overcome this obstacle, we apply the following method: First, when $k_\perp = 0$, $\bar{A}^{-a}(x^+, 0_\perp)$ can be generated by sampling a Gaussian random variable with the variance (note that we assume the QGP is overall color neutral $\langle \bar{A}^{-a} \rangle = 0$)

$$\langle \bar{A}^{-a}(x^+, 0_\perp) \bar{A}^{-a}(x^+, 0_\perp) \rangle = \gamma(0_\perp). \quad (3.31)$$

Next for $k_\perp \neq 0$, by using Eq. (3.30) we can show

$$\begin{aligned} \left\langle [\bar{A}^{-a}(x^+, k_\perp) + \bar{A}^{-a}(x^+, -k_\perp)] [\bar{A}^{-a}(x^+, k_\perp) + \bar{A}^{-a}(x^+, -k_\perp)] \right\rangle &= 2\gamma(\mathbf{k}_\perp), \\ \left\langle [i\bar{A}^{-a}(x^+, k_\perp) - i\bar{A}^{-a}(x^+, -k_\perp)] [i\bar{A}^{-a}(x^+, k_\perp) - i\bar{A}^{-a}(x^+, -k_\perp)] \right\rangle &= 2\gamma(\mathbf{k}_\perp), \end{aligned} \quad (3.32)$$

which means both $\bar{A}^{-a}(x^+, k_\perp) + \bar{A}^{-a}(x^+, -k_\perp)$ and $i\bar{A}^{-a}(x^+, k_\perp) - i\bar{A}^{-a}(x^+, -k_\perp)$ are Gaussian random variables with the variance $2\gamma(\mathbf{k}_\perp)$. We can then independently sample two Gaussian random variables X_1 and X_2 from a Gaussian distribution with the variance $2\gamma(\mathbf{k}_\perp)$ and finally obtain $(X_1 - iX_2)/2$ as the sampled classical background field.

This method requires $\mathcal{O}(tV_k)$ classical samplings to generate the random background fields for the construction of the quantum circuits describing the diffusion Hamiltonian evolution, where V_k denotes the volume of the momentum space, i.e., the number of lattice grids $V_k = N^+ N_\perp^2$. The quantum simulation with a given set of classical background fields corresponds to one particular trajectory for an initial state. In practice, one needs to repeat the classical sampling and the simulation of the diffusion process for multiple trajectories. Physical results are obtained by averaging over multiple trajectories. An interesting question is whether one can simulate the diffusion Hamiltonian evolution more efficiently by using some random quantum circuit [139] or modifying the Quantum Signal Processing algorithm [140, 141]. This is left for future studies.

4 Quantum Simulation of Toy Model

In this section we consider a simple toy model and demonstrate how to construct the quantum gates to describe the time evolution driven by the three pieces of the Hamiltonian, in order to study the LPM effect in jet quenching. We will also discuss how to generalize the construction for more complicated cases such as QCD. Then we will show some simulation results of the toy model that are obtained from the IBM Qiskit simulator.

4.1 Toy Model

The toy model we consider here is described by scalar fields in $2 + 1$ dimension with only $1 \rightarrow 2$ splitting and its inverse. In other words, we neglect the color, spin and q/g degrees of freedom discussed in the previous sections and focus on the case with only one transverse direction. With a limited number of qubits, we discretize the $+$ and \perp components of the momenta as

$$k^+ \in K_{\max}^+ \{0.5, 1\}, \quad k_{\perp} \in K_{\max}^{\perp} \{0, 1\}, \quad (4.1)$$

where k_{\perp} has only one component, rather than x and y components as in the previous sections. With more qubits available, one would add the second transverse component and further divide the momentum components into finer levels and eventually take the continuum limit. We will study the LPM effect in the case with one initial particle and only one splitting, which means the Hilbert space consists of 1-particle and 2-particle states. According to our discussion in Section 2.2, totally five qubits are needed to encode all quantum systems in this case. For each particle, we need one qubit to encode the transverse momentum and another for the $+$ component of the momentum. The correspondence between the qubit representation and the momentum state of a particle is given by

$$\begin{aligned} |00\rangle &: k^+ = 0.5, k_{\perp} = 0, \\ |01\rangle &: k^+ = 0.5, k_{\perp} = 1, \\ |10\rangle &: k^+ = 1, k_{\perp} = 0, \\ |11\rangle &: k^+ = 1, k_{\perp} = 1, \end{aligned} \quad (4.2)$$

where we have labeled the momenta by fractions of the maximum values. To encode both 1-particle and 2-particle states, we first need one qubit to distinguish them. Then we need another four qubits to represent the 2-particle states (representing the 1-particle states only requires two qubits). We list the values of the five qubits from left to right to describe a quantum state as $|q_1 q_2 q_3 q_4 q_5\rangle$. We use the following rules when encoding the states:

$$\left| \underbrace{q_1}_{\text{separate 1- and 2-particle states}} \underbrace{q_2 q_3}_{\text{describe momenta of the 2nd particle}} \underbrace{q_4 q_5}_{\text{describe momenta of the 1st particle}} \right\rangle, \quad (4.3)$$

where the momentum state of a particle is represented as in Eq. (4.2). In this way, the 1-particle state is represented as

$$|000q_4q_5\rangle, \quad (4.4)$$

where the second and the third 0s from the left have no physical meaning since this is a 1-particle state. On the other hand, the 2-particle state is labeled as

$$|1q_2q_3q_4q_5\rangle. \quad (4.5)$$

The setup can be easily generalized for multiple particles and cases requiring more qubits to represent 1-particle states such as those having more levels in the momentum description and degrees of freedom in color and spin: We will assign a certain number of qubits to label the number of particles in the state; Then for each particle, we will use a fixed number of qubits to represent its particle species, discretized momenta, color and spin degrees of freedom, as demonstrated in Eq. (4.3). This setup may not be the most efficient encoding scheme and other schemes should also be explored in the future.

4.2 Construction of Quantum Circuit

In general, when we have a matrix (H_{ij}) representing a given Hamiltonian H , we can construct the corresponding quantum gates by first projecting the matrix onto the basis made up of tensor products of Pauli matrices:

$$H = \sum_{\mu_1, \mu_2, \dots, \mu_n} a_{\mu_1 \mu_2 \dots \mu_n} \sigma_1^{\mu_1} \otimes \sigma_2^{\mu_2} \otimes \dots \otimes \sigma_n^{\mu_n}, \quad (4.6)$$

where we have assumed the matrix can be encoded by n qubits. Here $\sigma_i^{\mu_i}$ indicates the Pauli matrices for the i -th qubit and $\sigma^\mu = (\mathbb{1}, \sigma^x, \sigma^y, \sigma^z)$. The linear combination coefficients can be obtained by

$$a_{\mu_1 \mu_2 \dots \mu_n} = \frac{1}{2^n} \text{Tr} \left[H (\sigma_1^{\mu_1} \otimes \sigma_2^{\mu_2} \otimes \dots \otimes \sigma_n^{\mu_n}) \right], \quad (4.7)$$

where we have a matrix multiplication between H and $\sigma_1^{\mu_1} \otimes \sigma_2^{\mu_2} \otimes \dots \otimes \sigma_n^{\mu_n}$ inside the trace.

After obtaining the linear combination coefficients $a_{\mu_1 \mu_2 \dots \mu_n}$, we can construct the quantum gates for the time evolution $e^{-i\Delta t H}$. Using the Trotterization method, we can write

$$e^{-i\Delta t H} = e^{\mathcal{O}((\Delta t)^2)} \prod_{\mu_1, \mu_2, \dots, \mu_n} e^{-i\Delta t a_{\mu_1 \mu_2 \dots \mu_n} \sigma_1^{\mu_1} \otimes \sigma_2^{\mu_2} \otimes \dots \otimes \sigma_n^{\mu_n}}. \quad (4.8)$$

Therefore, once we know how to construct the quantum gates for the time evolution determined by one of the tensor products of Pauli matrices, we can construct the full time evolution determined by H . Without loss of generality, we discuss how to construct the quantum gates for

$$e^{-i\theta \sigma_1^{\mu_1} \otimes \sigma_2^{\mu_2} \otimes \dots \otimes \sigma_n^{\mu_n}}. \quad (4.9)$$

The strategy is to change the basis of each single qubit such that all the Pauli matrices $\sigma_i^{\mu_i}$ become either $\mathbb{1}_i$ or σ_i^z . If the original Pauli matrix $\sigma_i^{\mu_i} = \mathbb{1}_i$ or σ_i^z , nothing needs to be done for the i -th qubit. If the original Pauli matrix $\sigma_i^{\mu_i}$ is σ_i^x , then we apply the Hadamard gate

$$h = \frac{1}{\sqrt{2}} \begin{pmatrix} 1 & 1 \\ 1 & -1 \end{pmatrix}, \quad (4.10)$$

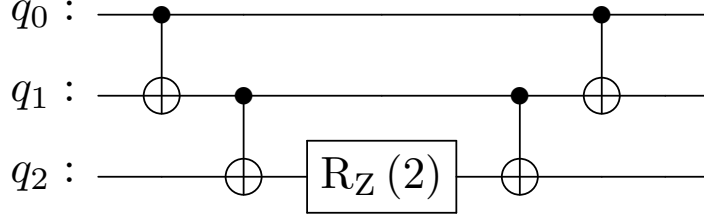


Figure 3: Quantum circuit for the unitary evolution $e^{-i\theta\sigma_1^z \otimes \sigma_2^z \otimes \sigma_3^z}$. Every two-qubit gate in the circuit is a CNOT gate with the black dot indicating the control qubit. The argument of the z -rotation represents the index of the qubit on which the rotation acts. The z -rotation gate is given by $R_z = e^{-i\theta\sigma_z} = \text{diag}(e^{-i\theta}, e^{+i\theta})$.

in the beginning and apply its inverse (which turns out to be itself) in the end of the circuit segment such that

$$h_i e^{-i\theta\sigma_i^x} h_i = e^{-i\theta\sigma_i^z}, \quad (4.11)$$

where the subscript i indicates the Hadamard gate acts on the i -th qubit. Similarly, if the original Pauli matrix is $\sigma_i^{\mu_i} = \sigma_i^y$, we apply

$$R_x = \frac{1}{\sqrt{2}} \begin{pmatrix} 1 & -i \\ -i & 1 \end{pmatrix}, \quad (4.12)$$

and its inverse in the beginning and the end of the circuit segment respectively such that

$$(R_x)_i e^{-i\theta\sigma_i^y} (R_x^\dagger)_i = e^{-i\theta\sigma_i^z}, \quad (4.13)$$

where the subscript i indicates the R_x rotation gate acts on the i -th qubit. The R_x rotation gate can be decomposed as

$$R_x = S^\dagger h S, \quad S = \begin{pmatrix} 1 & 0 \\ 0 & i \end{pmatrix}, \quad (4.14)$$

which can be useful in the construction of the quantum circuit.

In a nutshell, we only need to focus on constructing quantum gates for

$$e^{-i\theta\sigma_1^z \otimes \dots \otimes \sigma_m^z}, \quad (4.15)$$

where we have omitted the identity matrices and relabeled the indexes in the subscripts. Standard circuits exist to realize such unitary transformations. For example, the quantum circuit for $e^{-i\theta\sigma_1^z \otimes \sigma_2^z \otimes \sigma_3^z}$ is shown in Fig. 3, which can be easily generalized for more σ^z s.

Now we are ready to construct the quantum circuit for the time evolution of the toy model. We will show the quantum gates for the kinetic, diffusion and splitting terms in the Hamiltonian.

4.2.1 Kinetic Term

The kinetic term is diagonal in the n -particle basis we haven chosen, which means the decomposition of the kinetic Hamiltonian into tensor products of Pauli matrices only involves $\mathbb{1}_i$ and σ_i^z . We first construct the quantum circuit representing the 1-particle kinetic term, which only involves two qubits and will serve as a building block for the quantum circuit of the full kinetic term. In the basis given by Eq. (4.2), which is listed in the order $|00\rangle, |01\rangle, |10\rangle, |11\rangle$, the kinetic term is given by

$$H_{\text{kin}}^{(1)} = \frac{(K_{\text{max}}^\perp)^2}{K_{\text{max}}^+} \text{diag}(0, 2, 0, 1). \quad (4.16)$$

We decompose it into the format

$$H_{\text{kin}}^{(1)} = a_{11} \mathbb{1}_1 \otimes \mathbb{1}_2 + a_{1z} \mathbb{1}_1 \otimes \sigma_2^z + a_{z1} \sigma_1^z \otimes \mathbb{1}_2 + a_{zz} \sigma_1^z \otimes \sigma_2^z. \quad (4.17)$$

The linear combination coefficients can be easily found to be

$$a_{11} = \frac{3}{4} \frac{(K_{\text{max}}^\perp)^2}{K_{\text{max}}^+}, \quad a_{1z} = -\frac{3}{4} \frac{(K_{\text{max}}^\perp)^2}{K_{\text{max}}^+}, \quad a_{z1} = \frac{1}{4} \frac{(K_{\text{max}}^\perp)^2}{K_{\text{max}}^+}, \quad a_{zz} = -\frac{1}{4} \frac{(K_{\text{max}}^\perp)^2}{K_{\text{max}}^+}. \quad (4.18)$$

Our basis for the toy model consists of five qubits and contains both 1-particle and 2-particle states. We now discuss how to embed the decomposition (4.17) into the five qubit system. First, the 1-particle states in the five-qubit system have the first three qubits set to 0s, as shown in Eq. (4.4). So the 1-particle part of the kinetic Hamiltonian is represented as

$$H_{\text{kin}}^{(1)} = \frac{(K_{\text{max}}^\perp)^2}{K_{\text{max}}^+} \frac{\mathbb{1}_1 + \sigma_1^z}{2} \otimes \frac{\mathbb{1}_2 + \sigma_2^z}{2} \otimes \frac{\mathbb{1}_3 + \sigma_3^z}{2} \otimes \left(\frac{3}{4} \mathbb{1}_4 \otimes \mathbb{1}_5 - \frac{3}{4} \mathbb{1}_4 \otimes \sigma_5^z + \frac{1}{4} \sigma_4^z \otimes \mathbb{1}_5 - \frac{1}{4} \sigma_4^z \otimes \sigma_5^z \right), \quad (4.19)$$

where we abused the notation to use $H_{\text{kin}}^{(1)}$ again for the 1-particle states in the five-qubit system, which should be distinguished from that in Eq. (4.17) for the two-qubit system. The first three $\mathbb{1}_i + \sigma_i^z$ terms assure that $H_{\text{kin}}^{(1)}$ is nonvanishing only when the first three qubits are all 0s. In practice, when the first qubit is set to 0, i.e., the state is a 1-particle state, the second and third qubits will also be set to 0s. In other words, there is some redundancy in the five-qubit description of the 1-particle state. We can remove the redundancy in the qubit representation of the 1-particle kinetic Hamiltonian by using

$$H_{\text{kin}}^{(1)} = \frac{(K_{\text{max}}^\perp)^2}{K_{\text{max}}^+} \frac{\mathbb{1}_1 + \sigma_1^z}{2} \otimes \left(\frac{3}{4} \mathbb{1}_4 \otimes \mathbb{1}_5 - \frac{3}{4} \mathbb{1}_4 \otimes \sigma_5^z + \frac{1}{4} \sigma_4^z \otimes \mathbb{1}_5 - \frac{1}{4} \sigma_4^z \otimes \sigma_5^z \right), \quad (4.20)$$

which leads to a much simpler quantum circuit.

Next, we discuss the kinetic term for the 2-particle states in the five-qubit system. As Eq. (4.5) shows, the 2-particle states have the first qubit set to 1. So its kinetic Hamiltonian can be decomposed as

$$H_{\text{kin}}^{(2)} = \frac{(K_{\text{max}}^\perp)^2}{K_{\text{max}}^+} \frac{\mathbb{1}_1 - \sigma_1^z}{2} \otimes \left(\frac{3}{4} \mathbb{1}_2 \otimes \mathbb{1}_3 - \frac{3}{4} \mathbb{1}_2 \otimes \sigma_3^z + \frac{1}{4} \sigma_2^z \otimes \mathbb{1}_3 - \frac{1}{4} \sigma_2^z \otimes \sigma_3^z \right) \otimes \left(\frac{3}{4} \mathbb{1}_4 \otimes \mathbb{1}_5 - \frac{3}{4} \mathbb{1}_4 \otimes \sigma_5^z + \frac{1}{4} \sigma_4^z \otimes \mathbb{1}_5 - \frac{1}{4} \sigma_4^z \otimes \sigma_5^z \right), \quad (4.21)$$

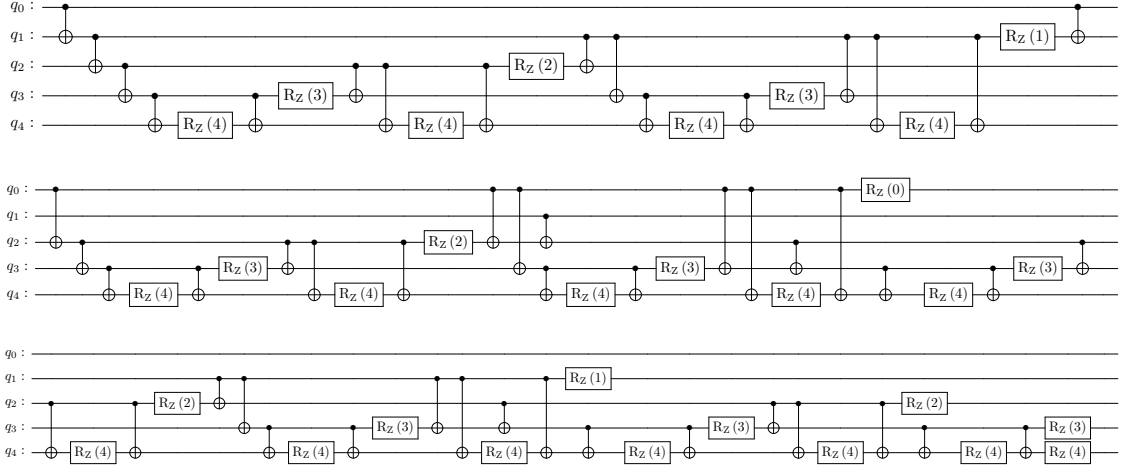


Figure 4: Quantum circuit for the time evolution determined by the kinetic part of the Hamiltonian. Every two-qubit gate in the circuit is a CNOT gate with the black dot indicating the control qubit. The argument of the z -rotation represents the index of the qubit on which the rotation acts. The z -rotation gate is given by $R_z = e^{-iC\Delta t \sigma_z (K_{\max}^\perp)^2 / (32K_{\max}^+)}$ with the constants C given in Eq. (4.22).

where the $\mathbb{1}_1 - \sigma_1^z$ term guarantees $H_{\text{kin}}^{(2)}$ is nonzero only when the first qubit is 1, i.e., the state is a 2-particle state.

The total kinetic Hamiltonian for the toy model is given by the sum $H_{\text{kin}} = H_{\text{kin}}^{(1)} + H_{\text{kin}}^{(2)}$. The quantum circuit to simulate the time evolution driven by the kinetic term can be constructed by using the method explained above. The identity operator $\mathbb{1}_1 \otimes \mathbb{1}_2 \otimes \mathbb{1}_3 \otimes \mathbb{1}_4 \otimes \mathbb{1}_5$ in the Hamiltonian only induces a global phase shift with no physical effect and thus can be neglected. Omitting identity operators and reorganizing lead to

$$\begin{aligned}
H_{\text{kin}} = \frac{(K_{\max}^\perp)^2}{32K_{\max}^+} & \left(-\sigma_1^z \otimes \sigma_2^z \otimes \sigma_3^z \otimes \sigma_4^z \otimes \sigma_5^z + \sigma_1^z \otimes \sigma_2^z \otimes \sigma_3^z \otimes \sigma_4^z - 3\sigma_1^z \otimes \sigma_2^z \otimes \sigma_3^z \otimes \sigma_5^z \right. \\
& + 3\sigma_1^z \otimes \sigma_2^z \otimes \sigma_3^z + \sigma_1^z \otimes \sigma_2^z \otimes \sigma_4^z \otimes \sigma_5^z - \sigma_1^z \otimes \sigma_2^z \otimes \sigma_4^z + 3\sigma_1^z \otimes \sigma_2^z \otimes \sigma_5^z - 3\sigma_1^z \otimes \sigma_2^z \\
& - 3\sigma_1^z \otimes \sigma_3^z \otimes \sigma_4^z \otimes \sigma_5^z + 3\sigma_1^z \otimes \sigma_3^z \otimes \sigma_4^z - 9\sigma_1^z \otimes \sigma_3^z \otimes \sigma_5^z + 9\sigma_1^z \otimes \sigma_3^z - \sigma_1^z \otimes \sigma_4^z \otimes \sigma_5^z \\
& + \sigma_1^z \otimes \sigma_4^z - 3\sigma_1^z \otimes \sigma_5^z + 3\sigma_1^z + \sigma_2^z \otimes \sigma_3^z \otimes \sigma_4^z \otimes \sigma_5^z - \sigma_2^z \otimes \sigma_3^z \otimes \sigma_4^z + 3\sigma_2^z \otimes \sigma_3^z \otimes \sigma_5^z \\
& - 3\sigma_2^z \otimes \sigma_3^z - \sigma_2^z \otimes \sigma_4^z \otimes \sigma_5^z + \sigma_2^z \otimes \sigma_4^z - 3\sigma_2^z \otimes \sigma_5^z + 3\sigma_2^z + 3\sigma_3^z \otimes \sigma_4^z \otimes \sigma_5^z - 3\sigma_3^z \otimes \sigma_4^z \\
& \left. + 9\sigma_3^z \otimes \sigma_5^z - 9\sigma_3^z - 7\sigma_4^z \otimes \sigma_5^z + 7\sigma_4^z - 21\sigma_5^z \right), \tag{4.22}
\end{aligned}$$

in which every term commutes with each other. The quantum circuit for the time evolution determined by the kinetic term $e^{-i\Delta t H_{\text{kin}}}$ is shown in Fig. 4.

4.2.2 Diffusion

The diffusion part of the Hamiltonian depends on an external classical background field, which is needed for the construction. Here we just assume the classical background fields at each momentum grid have been generated by using the sampling method described in Section 3.4

for each time step in the time evolution. For notational consistency, we still use \bar{A}^- to label the classical background fields here, even though our toy model has no gauge fields. Since our toy model has only two levels in the transverse momentum, we only need the classical background fields \bar{A}^- at two values of the transverse momenta 0 and K_{\max}^\perp . When the state is a 1-particle state, i.e., the first qubit in the register has a value of 0, the diffusion Hamiltonian only changes the last qubit in the register. This can be represented as

$$H_{\text{diff}}^{(1)} = g_d \frac{\mathbb{1}_1 + \sigma_1^z}{2} \otimes \left(\bar{A}^-(0) \mathbb{1}_5 + \bar{A}^-(K_{\max}^\perp) \sigma_5^x \right), \quad (4.23)$$

where g_d is the coupling strength. When the state is a 2-particle state, the diffusion can change both the third and the fifth qubits in the register. So we have

$$H_{\text{diff}}^{(2)} = g_d \frac{\mathbb{1}_1 - \sigma_1^z}{2} \otimes \left(\bar{A}^-(0) \mathbb{1}_3 \otimes \mathbb{1}_5 + \bar{A}^-(K_{\max}^\perp) \sigma_3^x \otimes \sigma_5^x \right). \quad (4.24)$$

The total Hamiltonian describing the transverse momentum diffusion is given by the sum:

$$H_{\text{diff}} = g_d \bar{A}^-(K_{\max}^\perp) \left(\frac{\mathbb{1}_1 + \sigma_1^z}{2} \otimes \sigma_5^x + \frac{\mathbb{1}_1 - \sigma_1^z}{2} \otimes \sigma_3^x \otimes \sigma_5^x \right), \quad (4.25)$$

where we have neglected the identity operator $g_d \bar{A}^-(0) \mathbb{1}_1 \otimes \mathbb{1}_3 \otimes \mathbb{1}_5$ which only leads to a global phase shift in the time evolution and contains no physics. Reorganizing leads to

$$H_{\text{diff}} = \frac{g_d}{2} \bar{A}^-(K_{\max}^\perp) \left(-\sigma_1^z \otimes \sigma_3^x \otimes \sigma_5^x + \sigma_1^z \otimes \sigma_5^x + \sigma_3^x \otimes \sigma_5^x + \sigma_5^x \right). \quad (4.26)$$

We want to emphasize again that the diffusion Hamiltonian H_{diff} is time dependent and the dependence is through the classical background field. The quantum circuit for the diffusion time evolution $e^{-i\Delta t H_{\text{diff}}}$ is depicted in Fig. 5. For general cases with more particles and more momenta levels, we will first construct the quantum gates describing the transverse momentum diffusion for 1-particle states, which corresponds to hoppings between different transverse momentum levels. Then we can use the quantum gates for the 1-particle transverse momentum diffusion as building blocks to construct the gates for the n -particle transverse momentum diffusion, as done above for the kinetic term.

4.2.3 Splitting

Finally we discuss the Pauli matrix representation of the splitting part of the Hamiltonian. Due to the momentum conservation in k^+ and k_\perp , only the following $1 \rightarrow 2$ splitting process can happen in our toy model:

$$\begin{aligned} |00010\rangle &\rightarrow |10000\rangle \\ |00011\rangle &\rightarrow |10001\rangle + |10100\rangle. \end{aligned} \quad (4.27)$$

In the first process, the initial particle with $k^+ = K_{\max}^+$ and $k_\perp = 0$ splits into two particles that both have $k^+ = 0.5K_{\max}^+$ and $k_\perp = 0$. In the second process, the initial particle with $k^+ = K_{\max}^+$ and $k_\perp = K_{\max}^\perp$ splits into two particles, one with $k^+ = 0.5K_{\max}^+$ and $k_\perp = 0$ and the other with $k^+ = 0.5K_{\max}^+$ and $k_\perp = K_{\max}^\perp$. The splitting process described in Eq. (4.27)

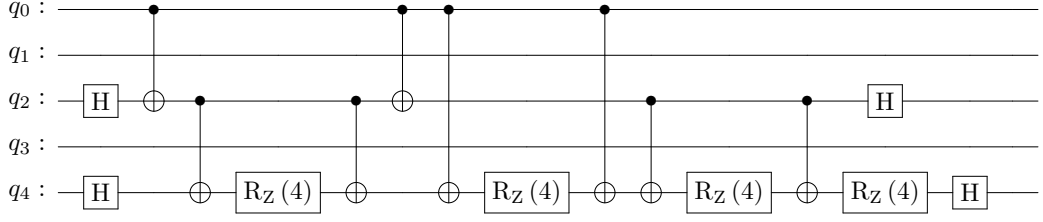


Figure 5: Quantum circuit for the time evolution driven by the diffusion part of the Hamiltonian. Every two-qubit gate in the circuit is a CNOT gate with the black dot indicating the control qubit. The argument of the z -rotation represents the index of the qubit on which the rotation acts. The z -rotation gate is given by $R_z = e^{\pm i g_d \bar{A}^-(K_{\max}^\perp) \Delta t \sigma_z / 2}$ and $\bar{A}^-(K_{\max}^\perp)$ is the time dependent classical background field.

symmetrizes the final state, up to a normalization. The Pauli matrix representation for the process described in Eq. (4.27) can be written as

$$\begin{aligned}
H_{\text{split}} &= g_s \left(\sigma_1^x \otimes \frac{\mathbb{1}_2 + \sigma_2^z}{2} \otimes \frac{\mathbb{1}_3 + \sigma_3^z}{2} \otimes \sigma_4^x \otimes \frac{\mathbb{1}_5 + \sigma_5^z}{2} + \sigma_1^x \otimes \frac{\mathbb{1}_2 + \sigma_2^z}{2} \otimes \frac{\mathbb{1}_3 + \sigma_3^z}{2} \right. \\
&\quad \left. \otimes \sigma_4^x \otimes \frac{\mathbb{1}_5 - \sigma_5^z}{2} + \sigma_1^x \otimes \frac{\mathbb{1}_2 + \sigma_2^z}{2} \otimes \sigma_3^x \otimes \sigma_4^x \otimes \sigma_5^x \right) \\
&= g_s \left(\sigma_1^x \otimes \frac{\mathbb{1}_2 + \sigma_2^z}{2} \otimes \frac{\mathbb{1}_3 + \sigma_3^z}{2} \otimes \sigma_4^x \otimes \mathbb{1}_5 + \sigma_1^x \otimes \frac{\mathbb{1}_2 + \sigma_2^z}{2} \otimes \sigma_3^x \otimes \sigma_4^x \otimes \sigma_5^x \right),
\end{aligned} \tag{4.28}$$

where the coupling strength g_s can in general depend on k^+ and k_\perp , as in the QCD case discussed in Section 3.3. The matrix of the splitting Hamiltonian is Hermitian, which means parton recombination has been accounted for. The splitting Hamiltonian can be decomposed into two non-commuting Hamiltonians $H_{\text{split}} = H_{\text{split}1} + H_{\text{split}2}$:

$$H_{\text{split}1} = \frac{g_s}{4} \left(\sigma_1^x \otimes \sigma_2^z \otimes \sigma_3^z \otimes \sigma_4^x + \sigma_1^x \otimes \sigma_2^z \otimes \sigma_4^x + \sigma_1^x \otimes \sigma_3^z \otimes \sigma_4^x + \sigma_1^x \otimes \sigma_4^x \right) \tag{4.29}$$

$$H_{\text{split}2} = \frac{g_s}{2} \left(\sigma_1^x \otimes \sigma_2^z \otimes \sigma_3^x \otimes \sigma_4^x \otimes \sigma_5^x + \sigma_1^x \otimes \sigma_3^x \otimes \sigma_4^x \otimes \sigma_5^x \right). \tag{4.30}$$

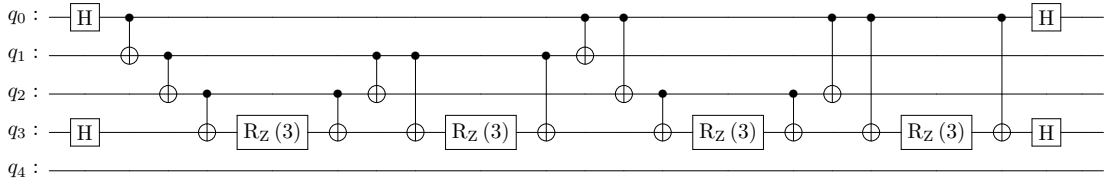
The quantum circuits for the time evolution determined by the two splitting parts of the Hamiltonian, i.e., $e^{-i\Delta t H_{\text{split}1}}$ and $e^{-i\Delta t H_{\text{split}2}}$ are given in Fig. 6.

This completes our construction of the quantum gates to describe the time evolution of the toy model.

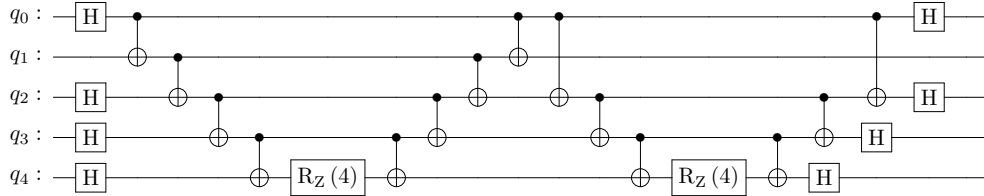
4.3 Simulation Results

Using the quantum circuits constructed above, we can now simulate the LPM effect in the toy model. We will perform the quantum simulation by using the Qiskit simulator package provided by IBM.

We will initialize the state as the 1-particle state with $k^+ = K_{\max}^+$ and $k_\perp = 0$, which is represented as $|00010\rangle$ in the quantum register. Since the quantum circuit constructed by the Qiskit package of IBM always initializes all the qubits to be in the 0 states, we still



(a) For H_{split1} with $R_z = e^{-ig_s \Delta t \sigma_z / 4}$.



(b) For H_{split2} with $R_z = e^{-ig_s \Delta t \sigma_z / 2}$.

Figure 6: Quantum circuits for the time evolution driven by the two splitting parts of the Hamiltonian. Every two-qubit gate in the circuit is a CNOT gate with the black dot indicating the control qubit. The argument of the z -rotation represents the index of the qubit on which the rotation acts.

need to apply the σ_4^x gate to obtain the initial state we want. After the state initialization, we evolve the state in time by using the quantum circuits constructed. In the end of the time evolution, we measure the first qubit. The result “0” in the measurement corresponds to a 1-particle state while the result “1” corresponds to a 2-particle state. The simulation and the measurement need repeating multiple times. Each repeating is called a shot.

The parameters are chosen as follows for the results we are going to show: $K_{\text{max}}^+ = 10$, $K_{\text{max}}^\perp = 1$, $g_d = 0.3$ and $g_s = 0.1$. The time evolution starts at $t = 0$ and ends at $t = 9$. We divide the time length to $N_t = 10$ steps for the Trotterization method. To study the LPM effect in the medium, we will compare the total radiation probability in vacuum with that in the medium. In the former case, the dynamics is described by the kinetic and splitting terms of the Hamiltonian $H_{\text{kin}} + H_{\text{split}}$, while in the latter, all three parts of the Hamiltonian $H_{\text{kin}} + H_{\text{diff}} + H_{\text{split}}$ are used in the description of the time evolution. For the in-medium simulation, we also need to average the results over multiple trajectories. For each trajectory, the classical background fields need regenerating. At each time step of a trajectory, we sample the classical background field $\bar{A}^-(K_{\text{max}}^+)$ by assuming it is described by a Gaussian distribution. The mean and the standard deviation of the Gaussian distribution are assumed to be 0 and 3 respectively.

The quantum simulation results of the total radiation probabilities are shown in Fig. 7 for the vacuum and medium cases, where the result “0” indicates that no radiation happens and the final state is still a 1-particle state while “1” represents that the $1 \rightarrow 2$ splitting occurs and the final state contains two particles. The vacuum result is obtained from 32768 shots while the medium result is obtained from averaging 500 trajectories. The result for

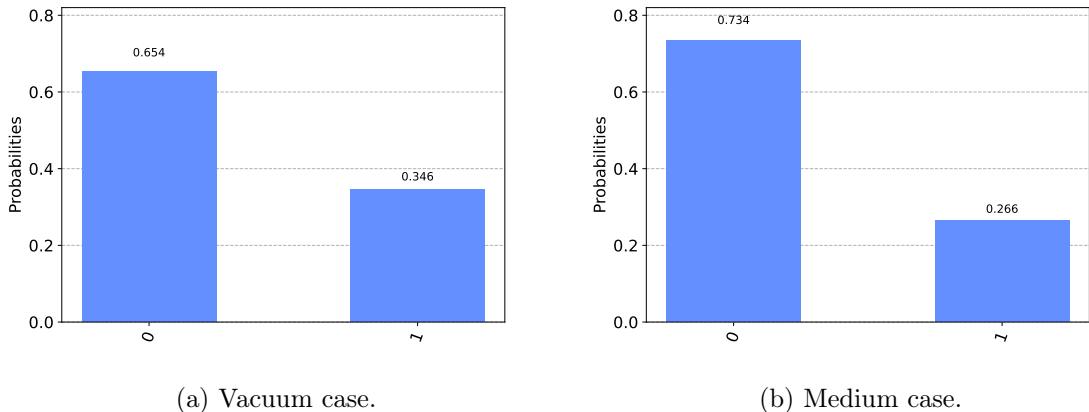


Figure 7: Quantum simulation results of the total radiation probabilities for the vacuum (left) and medium (right) cases. The measurement result “0” corresponds to no radiation while “1” indicates the occurrence of $1 \rightarrow 2$ splitting. The total radiation probability is suppressed in the medium case due to the LPM effect.

each trajectory is estimated from 32768 shots and every shot uses the same set of classical background fields sampled for the trajectory. It can be seen that once we turn on the diffusion Hamiltonian which originates from the transverse momentum exchange between partons and the medium, the radiation probability is suppressed. In other words, the LPM effect in radiation is observed in the quantum simulation of our toy model.

5 Conclusions

In this paper, we developed a framework to perform quantum simulation of jet quenching in nuclear environments. The quantum simulation automatically keeps track of quantum interference that is crucial in the studies of the LPM effect since it simulates the time evolution of a state wavefunction. We used the light-front Hamiltonian of QCD to describe the time evolution of high energy partons in the nuclear medium. The light-front Hamiltonian relevant for jet quenching consists of three pieces: a kinetic term which induces a phase change in the time evolution, a diffusion term caused by transverse momentum (Glauber) exchanges between the high energy partons and the medium, and a splitting term accounting for parton radiation and recombination. We use n -particle states in momentum space as the basis of the physical Hilbert space. In this basis, the kinetic Hamiltonian becomes diagonal, which can be efficiently simulated on a quantum computer. Furthermore, the matrices of the diffusion and splitting parts are sparse. Therefore, one may be able to efficiently simulate the LPM effect in jet quenching on a quantum computer. The diffusion term in the Hamiltonian depends on some classical background fields, of which the medium is a source. When constructing a quantum circuit for the Hamiltonian evolution, one needs to sample these classical background fields on a classical computer and then plug their values into the quantum circuit. This classical sampling scales as $\mathcal{O}(tV_k)$ where t is

the length of the time evolution and V_k is the volume of the momentum space. Quantum trajectories with different sets of classical background fields in the simulation need to be averaged to give estimates of physical results. Then we applied this framework to study the LPM effect in a toy model, by explicitly constructing a quantum circuit to simulate the time evolution. We observed the LPM effect in the toy model that suppresses the total radiation probability.

The framework developed here is general and it can be used to study the LPM effect in jet quenching for various media that are either static or expanding, thin or thick, hot or cold. It can also be applied for cases where the classical background fields satisfy some non-Gaussian correlations. Since the framework automatically keeps track of quantum interference, it can be applied to study the LPM effect with more than two splittings in a dynamically evolving medium, which is beyond the scope of state-of-the-art analyses. This framework of quantum simulation may help to deepen our understanding of jet quenching in nuclear environments in the near future with the advancement of quantum technology that provides more qubits of high fidelity, which is important for studies of jet production in current heavy ion collisions and in the forthcoming Electron-Ion Collider.

Acknowledgments

XY thanks Krishna Rajagopal and Martin Savage for useful discussions. The work of XY was supported by the U.S. Department of Energy, Office of Science, Office of Nuclear Physics grant DE-SC0011090.

A Light-Front Hamiltonian of QCD

We start with the QCD Lagrangian density with one massive fermion field

$$\mathcal{L} = \bar{\psi}(i\not{D} - m)\psi - \frac{1}{2}\text{Tr}(F^{\mu\nu}F_{\mu\nu}), \quad (\text{A.1})$$

where $\not{D} = \gamma^\mu D_\mu$, $D_\mu = \partial_\mu - igA_\mu$ and $F^{\mu\nu} = \frac{i}{g}[D^\mu, D^\nu]$. Writing the color indexes out explicitly leads to

$$\mathcal{L} = \bar{\psi}_i(i\not{D}_{ij} - m\delta_{ij})\psi_j - \frac{1}{4}F^{\mu\nu a}F_{\mu\nu}^a, \quad (\text{A.2})$$

where i, j, \dots denote the fundamental color indexes and a, b, \dots represent the adjoint color indexes and we have used $A^\mu = A^{\mu a}T^a$, $F^{\mu\nu a} = \partial^\mu A^{\nu a} - \partial^\nu A^{\mu a} + g^{abc}A^{\mu b}A^{\nu c}$ and $\text{Tr}(T^a T^b) = \frac{1}{2}\delta^{ab}$. Here we only raise and lower the Lorentz indexes but not the color indexes.

We will use the light-cone coordinates defined by

$$x^\pm = x^0 \pm x^3, \quad \gamma^\pm = \gamma^0 \pm \gamma^3, \quad A^\pm = A^0 \pm A^3, \quad (\text{A.3})$$

where x^+ denotes the light-cone time while x^- is the light-cone longitudinal coordinate. The metric is fixed as ($\mu = +, 1, 2, -$)

$$g_{\mu\nu} = \begin{pmatrix} 0 & 0 & 0 & \frac{1}{2} \\ 0 & -1 & 0 & 0 \\ 0 & 0 & -1 & 0 \\ \frac{1}{2} & 0 & 0 & 0 \end{pmatrix}, \quad g^{\mu\nu} = \begin{pmatrix} 0 & 0 & 0 & 2 \\ 0 & -1 & 0 & 0 \\ 0 & 0 & -1 & 0 \\ 2 & 0 & 0 & 0 \end{pmatrix}. \quad (\text{A.4})$$

The inner product between two vectors is given by

$$x \cdot y = x^\mu y_\mu = \frac{x^+ y^- + x^- y^+}{2} + \mathbf{x}_\perp \cdot \mathbf{y}_\perp = \frac{x^+ y^- + x^- y^+}{2} - \mathbf{x}_\perp \cdot \mathbf{y}_\perp. \quad (\text{A.5})$$

For the transverse components, we define the notation

$$x_\perp \cdot y_\perp = -\mathbf{x}_\perp \cdot \mathbf{y}_\perp = x_\perp^i y_{\perp i} = -x_{\perp i} y_{\perp i} = -x_\perp^i y_{\perp i}^i. \quad (\text{A.6})$$

The momentum component conjugated to x^+ is the light-cone energy p^- while the momentum component conjugated to x^- is the longitudinal momentum p^+ . From the on-shell condition $p^2 = m^2$, we find $p^- = (\mathbf{p}_\perp^2 + m^2)/p^+$. If p^+ is large, p^- will be small.

In the following, we will use light-cone gauge $A^+ = 0$ and derive the light-front Hamiltonian density defined by

$$\mathcal{H} = \sum_{\phi=\psi, A^\mu} \Pi_\phi \dot{\phi} - \mathcal{L}(\phi, \dot{\phi}), \quad (\text{A.7})$$

where the canonical momentum is given by

$$\Pi_\phi = \frac{\partial \mathcal{L}(\phi, \dot{\phi})}{\partial \dot{\phi}}. \quad (\text{A.8})$$

A.1 Fermion Sector

We will use the Dirac representation of the gamma matrices

$$\gamma^0 = \begin{pmatrix} 1 & 0 \\ 0 & -1 \end{pmatrix}, \quad \gamma^i = \begin{pmatrix} 0 & \sigma_i \\ -\sigma_i & 0 \end{pmatrix}, \quad \gamma^\pm = \begin{pmatrix} 1 & \pm \sigma_z \\ \mp \sigma_z & -1 \end{pmatrix}. \quad (\text{A.9})$$

We define two projection operators

$$\Lambda^+ = \frac{1}{2} \gamma^0 \gamma^+ = \frac{1}{4} \gamma^- \gamma^+, \quad \Lambda^- = \frac{1}{2} \gamma^0 \gamma^- = \frac{1}{4} \gamma^+ \gamma^-. \quad (\text{A.10})$$

Some useful identities are $(\gamma^\pm)^\dagger = \gamma^\mp$, $(\gamma^+)^2 = (\gamma^-)^2 = 0$, $\gamma^+ \gamma^- = 2\gamma^+ \gamma^0 = 2\gamma^0 \gamma^-$, $\gamma^- \gamma^+ = 2\gamma^- \gamma^0 = 2\gamma^0 \gamma^+$, $\gamma^+ \gamma^- \gamma^+ = 4\gamma^+$ and $\gamma^- \gamma^+ \gamma^- = 4\gamma^-$, with which one can easily show $(\Lambda^\pm)^\dagger = \Lambda^\pm$, $\Lambda^\pm \Lambda^\pm = \Lambda^\pm$ and $\Lambda^\pm \Lambda^\mp = 0$. Using the projection operators, we can decompose the fermion field

$$\psi = \psi_+ + \psi_- = \Lambda^+ \psi + \Lambda^- \psi, \quad (\text{A.11})$$

where the two fields are defined by $\psi_+^\dagger = \psi^\dagger \Lambda^+$ and $\psi_-^\dagger = \psi^\dagger \Lambda^-$ respectively.

The equation of motion for the fermion field $(i\mathcal{D}-m)\psi = 0$ can be written out explicitly as

$$\frac{1}{2}(\gamma^+ D^- + \gamma^- \partial^+)(\psi_+ + \psi_-) + (\mathcal{D}_\perp + im)(\psi_+ + \psi_-) = 0, \quad (\text{A.12})$$

where we have set $A^+ = 0$. Using $\gamma^+ \Lambda^- = \gamma^- \Lambda^+ = 0$ and multiplying both sides on the left by γ^0 , we find

$$D^- \psi_+ + \partial^+ \psi_- + \gamma^0(\mathcal{D}_\perp + im)(\psi_+ + \psi_-) = 0. \quad (\text{A.13})$$

Using $\Lambda^\pm \gamma^0 \Lambda^\pm = 0$ and $\Lambda^\pm \gamma^0 \gamma_\perp \Lambda^\pm = 0$, we can project Eq. (A.13) onto the two fermion field components ψ_\pm and obtain

$$\begin{aligned} D^- \psi_+ + \gamma^0(\mathcal{D}_\perp + im)\psi_- &= 0, \\ \partial^+ \psi_- + \gamma^0(\mathcal{D}_\perp + im)\psi_+ &= 0. \end{aligned} \quad (\text{A.14})$$

The derivative ∂^- is with respect to the light-cone time while the derivative ∂^+ is with respect to the longitudinal coordinate. So we can solve ψ_- in terms of the ψ_+ at the same light-cone time

$$\psi_- = -\frac{1}{\partial^+} \gamma^0(\mathcal{D}_\perp + im)\psi_+. \quad (\text{A.15})$$

In other words, the ψ_- field is not dynamical. Plugging Eq. (A.15) into Eq. (A.14), we find the equation of motion for the ψ_+ field is given by

$$\partial^- \psi_+ - igA^- \psi_+ - \gamma^0(\mathcal{D}_\perp + im) \frac{1}{\partial^+} \gamma^0(\mathcal{D}_\perp + im)\psi_+ = 0. \quad (\text{A.16})$$

Since $\partial^- = \frac{\partial}{\partial^+}$ is the derivative with respect to the light-cone time, ψ_+ is a dynamical degree of freedom.

Using the identities shown above, we can write the fermionic part of the Lagrangian density in light-cone gauge as

$$\begin{aligned} \mathcal{L}_f &= i(\psi_+^\dagger D^- \psi_+ + \psi_-^\dagger \partial^+ \psi_- + \psi_-^\dagger \gamma^0(\mathcal{D}_\perp + im)\psi_+ + \psi_+^\dagger \gamma^0(\mathcal{D}_\perp + im)\psi_-) \\ &= i(\psi_+^\dagger D^- \psi_+ - \psi_+^\dagger \gamma^0(\mathcal{D}_\perp + im) \frac{1}{\partial^+} \gamma^0(\mathcal{D}_\perp + im)\psi_+), \end{aligned} \quad (\text{A.17})$$

where we have used Eq. (A.15). Then the fermionic part of the Hamiltonian density in light-cone gauge is given by

$$\mathcal{H}_f = -g\psi_+^\dagger A^- \psi_+ + i\psi_+^\dagger \gamma^0(\mathcal{D}_\perp + im) \frac{1}{\partial^+} \gamma^0(\mathcal{D}_\perp + im)\psi_+. \quad (\text{A.18})$$

To quantize the theory canonically, we decompose the ψ_+ field as

$$\psi_+^i(x^+ = 0, x_\perp, x^-) = \sum_{\sigma=\pm\frac{1}{2}} \int_{k^+>0} \frac{dk^+ d^2k_\perp}{2(2\pi)^3 k^+} \left(b^i(k, \sigma) u_+(k, \sigma) e^{-ik \cdot x} + d^{i\dagger}(k, \sigma) v_+(k, \sigma) e^{ik \cdot x} \right), \quad (\text{A.19})$$

where i is the color index in the fundamental representation and the quark (antiquark) creation $b^{i\dagger}(d^{i\dagger})$ and annihilation $b^i(d^i)$ operators satisfy the anticommutation relations

$$\{b^i(k, \sigma), b^{j\dagger}(k', \sigma')\} = \{d^i(k, \sigma), d^{j\dagger}(k', \sigma')\} = 2(2\pi)^3 k^+ \delta^{ij} \delta_{\sigma\sigma'} \delta^3(k - k'), \quad (\text{A.20})$$

and all the other anticommutators vanish. Here $\delta^3(k) = \delta(k^+) \delta^2(k_\perp)$. Using $u_+ = \Lambda_+ u$ and $\bar{u}_+ = \bar{u} \Lambda_-$, one can easily show

$$\sum_{\sigma=\pm\frac{1}{2}} u_+(k, \sigma) \bar{u}_+(k, \sigma) = \Lambda_+ \left(\sum_{\sigma=\pm\frac{1}{2}} u(k, \sigma) \bar{u}(k, \sigma) \right) \Lambda_- = \Lambda_+ \not{k} \Lambda_- = k^+ \Lambda_+ \gamma^0. \quad (\text{A.21})$$

So we have

$$\sum_{\sigma=\pm\frac{1}{2}} u_+(k, \sigma) u_+^\dagger(k, \sigma) = k^+ \Lambda_+, \quad \sum_{\sigma=\pm\frac{1}{2}} v_+(k, \sigma) v_+^\dagger(k, \sigma) = k^+ \Lambda_+. \quad (\text{A.22})$$

With these we can show the quark field satisfies the following anticommutation relation

$$\{\psi_+^i(x), \psi_+^{j\dagger}(y)\}_{x^+=y^+=0} = \Lambda_+ \delta^{ij} \delta^3(x - y), \quad (\text{A.23})$$

where the delta function in space is defined as $\delta^3(x) = \delta(x^-) \delta^2(x_\perp)$. Furthermore, from $\bar{u}(k, \sigma) \gamma^\mu u(k, \sigma') = 2p^\mu \delta_{\sigma\sigma'} = \bar{v}(k, \sigma) \gamma^\mu v(k, \sigma')$, we can show

$$u_+^\dagger(k, \sigma) u_+(k, \sigma') = \frac{1}{2} u^\dagger(k, \sigma) \gamma^0 \gamma^+ u(k, \sigma') = k^+ \delta_{\sigma\sigma'}, \quad v_+^\dagger(k, \sigma) v_+(k, \sigma') = k^+ \delta_{\sigma\sigma'}. \quad (\text{A.24})$$

The kinetic term in the fermionic part of the Hamiltonian can be worked out to give

$$\begin{aligned} H_{f, \text{kin}} &= \int d^3x \left(i \psi_+^\dagger \gamma^0 (\not{\partial}_\perp + im) \frac{1}{\partial^+} \gamma^0 (\not{\partial}_\perp + im) \psi_+ \right) \\ &= \int dx^- d^2x_\perp \left(i \psi_+^\dagger \frac{\not{\partial}_\perp^2 - m^2}{\partial^+} \psi_+ \right) \\ &= \sum_i \sum_{\sigma=\pm\frac{1}{2}} \sum_{\sigma'=\pm\frac{1}{2}} \int_{k^+>0} \frac{dk^+ d^2k_\perp}{2(2\pi)^3 k^+} \frac{\mathbf{k}_\perp^2 + m^2}{(k^+)^2} \left(b^{i\dagger}(k, \sigma) b^i(k, \sigma') u_+^\dagger(k, \sigma) u_+(k, \sigma') \right. \\ &\quad \left. - d^i(k, \sigma) d^{i\dagger}(k, \sigma') v_+^\dagger(k, \sigma) v_+(k, \sigma') \right) \\ &= \sum_i \sum_{\sigma=\pm\frac{1}{2}} \int_{k^+>0} \frac{dk^+ d^2k_\perp}{2(2\pi)^3 k^+} \frac{\mathbf{k}_\perp^2 + m^2}{k^+} \left(b^{i\dagger}(k, \sigma) b^i(k, \sigma) + d^{i\dagger}(k, \sigma) d^i(k, \sigma) \right) + \text{const}, \end{aligned} \quad (\text{A.25})$$

where we have used $d^3x = dx^- d^2x_\perp$, $\partial_\perp^2 = -\not{\partial}_\perp^2$, Eq. (A.24) and

$$\int_{k_1^+>0} dk_1^+ \int_{k_2^+>0} dk_2^+ \delta(k_1^+ + k_2^+) = 0. \quad (\text{A.26})$$

A.2 Gauge Sector

The gauge part of the Lagrangian density is given by

$$\mathcal{L}_g = -\frac{1}{4}F^{\mu\nu a}F_{\mu\nu}^a + g\bar{\psi}A\psi, \quad (\text{A.27})$$

where $F^{\mu\nu a} = \partial^\mu A^{\nu a} - \partial^\nu A^{\mu a} + gf^{abc}A^{\mu b}A^{\nu c}$. The equation of motion is determined from the Lagrangian equation

$$\frac{\partial\mathcal{L}_g}{\partial A^{\nu a}} = \partial^\mu \frac{\partial\mathcal{L}_g}{\partial(\partial^\mu A^{\nu a})}, \quad (\text{A.28})$$

which leads to

$$-g\bar{\psi}\gamma_\nu T^a\psi + gf^{abc}F_{\mu\nu}^b A^{\mu c} = \partial^\mu F_{\mu\nu}^a. \quad (\text{A.29})$$

In light-cone gauge $A^+ = 0$ and for $\nu = +$ (we raise ν to an upper index), using

$$F^{++a} = 0, \quad F^{-+a} = -\partial^+ A^{-a}, \quad F^{i+a} = -\partial^+ A_\perp^{ia}, \quad (\text{A.30})$$

we obtain

$$-g\bar{\psi}\gamma^+ T^a\psi + gf^{abc}F_i^{+b}A_\perp^{ic} = \frac{1}{2}\partial^+ F^{-+a} + \partial^i F_i^{+a}, \quad (\text{A.31})$$

which is simplified to be

$$-2g\psi_+^\dagger T^a\psi_+ + gf^{abc}(\partial^+ A_\perp^{ib})A_\perp^{ic} = \frac{1}{2}\partial^+(-\partial^+ A^{-a}) + \partial^i \partial^+ A_\perp^{ia}. \quad (\text{A.32})$$

Since the derivative ∂^+ is with respect to the longitudinal coordinate, we can invert Eq. (A.32) to obtain

$$A^{-a} = \frac{2}{\partial^+} \partial^i A_\perp^{ia} - \frac{2g}{\partial^{+2}} \left(f^{abc}(\partial^+ A_\perp^{ib})A_\perp^{ic} - 2\psi_+^\dagger T^a\psi_+ \right). \quad (\text{A.33})$$

As a result the A^{-a} is determined by the transverse components and thus not a dynamical degree of freedom. Since we have chosen $A^+ = 0$ in light-cone gauge, only two field degrees of freedom are left in the gauge part, i.e., A_\perp . We choose the two gluon polarization vectors to be (the determination of the transverse plane relies on choosing the $+$ and $-$ directions of the spacetime)

$$\varepsilon_\perp(\pm) = \frac{1}{\sqrt{2}}(1, \pm i), \quad (\text{A.34})$$

which satisfies the completeness relation

$$\sum_{\lambda=\pm} \varepsilon_\perp^\mu(\lambda)\varepsilon_\perp^{\nu*}(\lambda) = -g_\perp^{\mu\nu}, \quad \sum_{i=1,2} \varepsilon_\perp^i(\lambda_1)\varepsilon_\perp^{i*}(\lambda_2) = \delta_{\lambda_1\lambda_2}. \quad (\text{A.35})$$

The four component polarization vector ε^μ can be chosen to be

$$\varepsilon^+ = 0, \quad \varepsilon^- = -\frac{2k_\perp \cdot \varepsilon_\perp}{k^+}. \quad (\text{A.36})$$

The canonical momentum conjugated to the gauge field A_{\perp}^{ia} is given by

$$\Pi_{A_{\perp}^{ia}} = \frac{\partial \mathcal{L}}{\partial(\partial^{-} A_{\perp}^{ia})} = -\frac{1}{2} \partial^{+} A_{\perp i}^a = -\partial^{-} A_{\perp i}^a. \quad (\text{A.37})$$

Then the gauge part of the Hamiltonian density in light-cone gauge is given by

$$\begin{aligned} \mathcal{H}_g &= -\frac{1}{2} (\partial^{+} A_{\perp i}^a) (\partial^{-} A_{\perp}^{ia}) - \mathcal{L}_g \\ &= -\frac{1}{8} (\partial^{+} A^{-a})^2 + \frac{1}{2} (\partial^{+} A_{\perp}^{ia}) (-\partial_i A^{-a} + g f^{abc} A^{-b} A_{\perp i}^c) + \frac{1}{4} F_{\perp}^{ija} F_{\perp ij}^a, \end{aligned} \quad (\text{A.38})$$

where the A^{-a} component is fixed by Eq. (A.33). In canonical quantization, the gauge field is decomposed as

$$A_{\perp}^{ib}(x^{+} = 0, x_{\perp}, x^{-}) = \sum_{\lambda=\pm} \int_{k^{+}>0} \frac{dk^{+} d^2 k_{\perp}}{2(2\pi)^3 k^{+}} \left(a^b(k, \lambda) \varepsilon_{\perp}^i(\lambda) e^{-ik \cdot x} + a^{b\dagger}(k, \lambda) \varepsilon_{\perp}^{i*}(\lambda) e^{ik \cdot x} \right), \quad (\text{A.39})$$

in which $i = 1, 2$ denotes the transverse coordinate components and the gluon creation and annihilation operators satisfy the commutation relation

$$[a^b(k, \lambda), a^{c\dagger}(k', \lambda')] = 2(2\pi)^3 k^{+} \delta_{\lambda\lambda'} \delta^{bc} \delta^3(k - k'). \quad (\text{A.40})$$

Then one can show the commutation relation for the gauge fields

$$[A_{\perp}^{ib}(x), \partial^{+} A_{\perp}^{jc}(y)]_{x^{+}=y^{+}=0} = i \delta^{ij} \delta^{bc} \delta^3(x - y). \quad (\text{A.41})$$

The kinematic term in the gluon part of the Hamiltonian can be obtained by plugging Eq. (A.33) into Eq. (A.38) and neglecting all interaction terms, which leads to

$$\begin{aligned} H_{g, \text{kin}} &= \int dx^{-} d^2 x_{\perp} \left(-\frac{1}{2} (\partial^i A_{\perp}^{ia}) (\partial^j A_{\perp}^{ja}) - (\partial^{+} A_{\perp}^{ia}) (\partial_i \frac{1}{\partial^{+}} \partial^j A_{\perp}^{ja}) \right. \\ &\quad \left. + \frac{1}{2} (\partial^i A_{\perp}^{ja}) (\partial_i A_{\perp j}^a) - \frac{1}{2} (\partial^i A_{\perp}^{ja}) (\partial_j A_{\perp i}^a) \right) \\ &= \frac{1}{2} \int dx^{-} d^2 x_{\perp} (\partial^i A_{\perp}^{ja}) (\partial^i A_{\perp}^{ja}) \\ &= \sum_b \sum_{i=1,2} \sum_{\lambda_1=\pm} \sum_{\lambda_2=\pm} \int_{k^{+}>0} \frac{dk^{+} d^2 k_{\perp}}{2(2\pi)^3 k^{+}} \frac{\mathbf{k}_{\perp}^2}{2k^{+}} \left(a^b(k, \lambda_1) a^{b\dagger}(k, \lambda_2) \varepsilon_{\perp}^i(k, \lambda_1) \varepsilon_{\perp}^{i*}(k, \lambda_2) \right. \\ &\quad \left. + a^{b\dagger}(k, \lambda_1) a^b(k, \lambda_2) \varepsilon_{\perp}^{i*}(k, \lambda_1) \varepsilon_{\perp}^i(k, \lambda_2) \right) \\ &= \sum_b \sum_{\lambda=\pm} \int_{k^{+}>0} \frac{dk^{+} d^2 k_{\perp}}{2(2\pi)^3 k^{+}} \frac{\mathbf{k}_{\perp}^2}{k^{+}} a^{b\dagger}(k, \lambda) a^b(k, \lambda) + \text{const}, \end{aligned} \quad (\text{A.42})$$

where we have used Eq. (A.26) again.

A.3 Splitting

The total Hamiltonian density is $\mathcal{H} = \mathcal{H}_q + \mathcal{H}_g$ where \mathcal{H}_q and \mathcal{H}_g are given by Eqs. (A.18) and (A.38) respectively. Now we organize the part of the Hamiltonian relevant for splitting in powers of g and $\frac{1}{\partial^+}$. For the $i\psi_+^\dagger\gamma^0(\not{D}_\perp + im)\frac{1}{\partial^+}\gamma^0(\not{D}_\perp + im)\psi_+$, we find

$$\begin{aligned} \mathcal{O}\left(\frac{g}{\partial^+}\right) : & \quad -g\psi_+^\dagger A_{\perp i}\gamma^i\frac{1}{\partial^+}(\partial_{\perp j}\gamma^j + im)\psi_+ - g\psi_+^\dagger(\partial_{\perp i}\gamma^i - im)\frac{1}{\partial^+}(A_{\perp j}\gamma^j\psi_+) \quad (\text{A.43}) \\ & = -g\psi_+^\dagger A_{\perp i}\gamma^i\gamma^j\left(\frac{\partial_{\perp j}}{\partial^+}\psi_+\right) - g\left(\frac{\partial_{\perp i}}{\partial^+}\psi_+^\dagger\right)A_{\perp j}\gamma^i\gamma^j\psi_+ \\ & \quad - img\left(\psi_+^\dagger A_{\perp}\frac{1}{\partial^+}\psi_+ - \psi_+^\dagger\frac{1}{\partial^+}(A_{\perp}\psi_+)\right), \\ \mathcal{O}\left(\frac{g^2}{\partial^+}\right) : & \quad ig^2\psi_+^\dagger\gamma^j\gamma^j A_{\perp i}\frac{1}{\partial^+}(A_{\perp j}\psi_+), \end{aligned}$$

where we follow a notation that derivatives inside parentheses act on everything on their right inside the same parentheses, while if there are no parentheses, derivatives act on everything on their right. The term $-g\psi_+^\dagger A^- \psi_+$ with Eq. (A.33) leads to

$$\begin{aligned} \mathcal{O}\left(\frac{g}{\partial^+}\right) : & \quad -2g\psi_+^\dagger T^a\psi_+\left(\frac{\partial^i}{\partial^+}A_{\perp}^{ia}\right), \quad (\text{A.44}) \\ \mathcal{O}\left(\frac{g^2}{\partial^+}\right) : & \quad 2g^2 f^{abc}\psi_+^\dagger T^a\psi_+\left(\frac{1}{\partial^{+2}}(\partial^+ A_{\perp}^{ib})A_{\perp}^{ic}\right), \\ \mathcal{O}\left(\frac{g^2}{\partial^{+2}}\right) : & \quad -4g^2\psi_+^\dagger T^a\psi_+\left(\frac{1}{\partial^{+2}}\psi_+^\dagger T^a\psi_+\right). \end{aligned}$$

Next the term $-\frac{1}{8}(\partial^+ A^{-a})^2$ with Eq. (A.33) gives

$$\begin{aligned} \mathcal{O}(g) : & \quad gf^{abc}(\partial^i A_{\perp}^{ia})\left(\frac{1}{\partial^+}(\partial^+ A_{\perp}^{jb})A_{\perp}^{jc}\right) = -gf^{abc}\left(\frac{\partial^i}{\partial^+}A_{\perp}^{ia}\right)(\partial^+ A_{\perp}^{jb})A_{\perp}^{jc}, \quad (\text{A.45}) \\ \mathcal{O}\left(\frac{g}{\partial^+}\right) : & \quad -2g(\partial^i A_{\perp}^{ia})\left(\frac{1}{\partial^+}\psi_+^\dagger T^a\psi_+\right), \\ \mathcal{O}(g^2) : & \quad -\frac{g^2}{2}\left(f^{abc}\frac{1}{\partial^+}(\partial^+ A_{\perp}^{ib})A_{\perp}^{ic}\right)^2, \\ \mathcal{O}\left(\frac{g^2}{\partial^+}\right) : & \quad 2g^2 f^{abc}\left(\frac{1}{\partial^+}\psi_+^\dagger T^a\psi_+\right)\left(\frac{1}{\partial^+}(\partial^+ A_{\perp}^{ib})A_{\perp}^{ic}\right), \\ \mathcal{O}\left(\frac{g^2}{\partial^{+2}}\right) : & \quad -2g^2\left(\frac{1}{\partial^+}\psi_+^\dagger T^a\psi_+\right)^2. \end{aligned}$$

Furthermore, we find the term $-\frac{1}{2}(\partial^+ A_{\perp}^{ia})(\partial_i A^{-a})$ contributes as

$$\begin{aligned} \mathcal{O}(g) : & \quad gf^{abc}(\partial_i A_{\perp}^{ia})\left(\frac{1}{\partial^+}(\partial^+ A_{\perp}^{jb})A_{\perp}^{jc}\right) = gf^{abc}\left(\frac{\partial^i}{\partial^+}A_{\perp}^{ia}\right)(\partial^+ A_{\perp}^{jb})A_{\perp}^{jc}, \quad (\text{A.46}) \\ \mathcal{O}\left(\frac{g}{\partial^+}\right) : & \quad -2g(\partial_i A_{\perp}^{ia})\left(\frac{1}{\partial^+}\psi_+^\dagger T^a\psi_+\right). \end{aligned}$$

Then we obtain the contribution from the $\frac{1}{2}g f^{abc}(\partial^+ A_{\perp}^{ia})A^{-b}A_{\perp i}^c$ term

$$\begin{aligned}\mathcal{O}(g) &: g f^{abc}(\partial^+ A_{\perp}^{ia})\left(\frac{\partial^j}{\partial^+} A_{\perp}^{jb}\right)A_{\perp i}^c, \\ \mathcal{O}(g^2) &: -g^2 f^{abc} f^{bde}(\partial^+ A_{\perp}^{ia})\left(\frac{1}{\partial^{+2}}(\partial^+ A_{\perp}^{jd})A_{\perp}^{je}\right)A_{\perp i}^c, \\ \mathcal{O}\left(\frac{g^2}{\partial^+}\right) &: 2g^2 f^{abc}(\partial^+ A_{\perp}^{ia})\left(\frac{1}{\partial^{+2}}\psi_+^\dagger T^b \psi_+\right)A_{\perp i}^c.\end{aligned}\tag{A.47}$$

Finally, the term $-\frac{1}{4}F_{\perp}^{ija}F_{\perp ij}^a$ leads to

$$\begin{aligned}\mathcal{O}(g) &: -g f^{abc}(\partial^i A_{\perp}^{ja})A_{\perp i}^b A_{\perp j}^c, \\ \mathcal{O}(g^2) &: -\frac{1}{4}g^2 f^{abc} f^{ade}A_{\perp}^{ib}A_{\perp}^{jc}A_{\perp i}^d A_{\perp j}^e.\end{aligned}\tag{A.48}$$

B Phase Kickback Method

The phase kickback method has been used in the quantum simulation of scalar field theory [117, 118]. Without loss of generality, consider a n -particle state

$$|p\rangle = \prod_{i=1}^n |p_i^+, p_i^x, p_i^y, \dots\rangle, \tag{B.1}$$

where the dots represent other degrees of freedom such as colors and spins that are irrelevant for the kinetic energy evolution. The kinetic energy evolution in a small time step Δt is given by

$$\begin{aligned}e^{-iH_{\text{kin}}\Delta t}|p\rangle &= e^{i2\pi f(p)}|p\rangle, \\ f(p) &= -\frac{\Delta t}{2\pi} \sum_{i=1}^n \frac{\mathbf{p}_{i\perp}^2}{p_i^+} \theta(p_i^+),\end{aligned}\tag{B.2}$$

where the θ function assures that unphysical states do not contribute to the phase. The phase $f(p)$ can be represented in a binary representation:

$$f(p) = \sum_{m=-\infty}^{+\infty} f_m(p)2^m, \tag{B.3}$$

where $f_m(p) = 0, 1$. The terms with $m \geq 0$ are irrelevant since $e^{-i2\pi n} = 1$ for any integer n . Suppose we want to implement the phase rotation with a precision to the N th binary decimal, i.e.,

$$f(p) \approx \sum_{m=-N}^{-1} f_m(p)2^m = \frac{1}{2^N} \sum_{j=0}^{N-1} f_{j-N}(p)2^j \equiv \frac{1}{2^N} \tilde{f}(p). \tag{B.4}$$

We have defined a ‘‘discretized’’ phase factor $\tilde{f}(p)$ that outputs integers in $\{0, 1, 2, \dots, 2^N - 1\}$. In general the map \tilde{f} is not injective, so one cannot construct a unitary operator $V_{\tilde{f}}$

such that $V_{\tilde{f}}|p\rangle = |\tilde{f}(p)\rangle$. However, it is always possible to define a unitary operator $U_{\tilde{f}}$ such that [142]

$$U_{\tilde{f}}(|p\rangle \otimes |j\rangle) = |p\rangle \otimes |j + \tilde{f}(p) \bmod 2^N\rangle, \quad (\text{B.5})$$

for $j \in \{0, 1, 2, \dots, 2^N - 1\}$ as an auxiliary register. The number of quantum gates needed to implement this unitary operator is only larger than that of the classical gates by at most a constant factor [142]. If the auxiliary register is initialized to be

$$|s\rangle = \frac{1}{\sqrt{2^N}} \sum_{j=0}^{2^N-1} e^{-2\pi i j/2^N} |j\rangle, \quad (\text{B.6})$$

where $|j\rangle$ is the computational basis of the auxiliary register, i.e., $|j\rangle = |000 \dots 00\rangle, |000 \dots 01\rangle, |000 \dots 10\rangle, \dots$, in each of which we have N binary numbers, we can apply the unitary operator defined in Eq. (B.5) to $|p\rangle \otimes |s\rangle$ to obtain

$$\begin{aligned} U_{\tilde{f}}(|p\rangle \otimes |s\rangle) &= |p\rangle \otimes \frac{1}{\sqrt{2^N}} \sum_{j=0}^{2^N-1} e^{-2\pi i j/2^N} |j + \tilde{f}(p) \bmod 2^N\rangle \\ &= |p\rangle \otimes \frac{1}{\sqrt{2^N}} \sum_{k=0}^{2^N-1} e^{i2\pi \tilde{f}(p)} e^{-2\pi i k/2^N} |k\rangle \\ &= e^{i2\pi \tilde{f}(p)} |p\rangle \otimes |s\rangle. \end{aligned} \quad (\text{B.7})$$

In this way we have realized the phase rotation that we want to apply to the state $|p\rangle$. The initial auxiliary register $|s\rangle$ in Eq. (B.6) can be efficiently prepared by applying the Quantum Fourier Transform to the state $|j = 1\rangle$ in the register.

References

- [1] J. M. Butterworth, A. R. Davison, M. Rubin and G. P. Salam, *Jet substructure as a new Higgs search channel at the LHC*, *Phys.Rev.Lett.* **100** (2008) 242001, [[0802.2470](#)].
- [2] S. D. Ellis, C. K. Vermilion and J. R. Walsh, *Techniques for improved heavy particle searches with jet substructure*, *Phys.Rev.* **D80** (2009) 051501, [[0903.5081](#)].
- [3] I. W. Stewart, F. J. Tackmann and W. J. Waalewijn, *N-Jettiness: An Inclusive Event Shape to Veto Jets*, *Phys. Rev. Lett.* **105** (2010) 092002, [[1004.2489](#)].
- [4] S. D. Ellis, C. K. Vermilion, J. R. Walsh, A. Hornig and C. Lee, *Jet Shapes and Jet Algorithms in SCET*, *JHEP* **1011** (2010) 101, [[1001.0014](#)].
- [5] A. Abdesselam et al., *Boosted objects: A Probe of beyond the Standard Model physics*, *Eur. Phys. J.* **C71** (2011) 1661, [[1012.5412](#)].
- [6] A. Altheimer et al., *Jet Substructure at the Tevatron and LHC: New results, new tools, new benchmarks*, *J. Phys.* **G39** (2012) 063001, [[1201.0008](#)].
- [7] A. J. Larkoski, G. P. Salam and J. Thaler, *Energy Correlation Functions for Jet Substructure*, *JHEP* **06** (2013) 108, [[1305.0007](#)].

- [8] A. Altheimer et al., *Boosted objects and jet substructure at the LHC. Report of BOOST2012, held at IFIC Valencia, 23rd-27th of July 2012*, *Eur. Phys. J.* **C74** (2014) 2792, [[1311.2708](#)].
- [9] M. Dasgupta, A. Fregoso, S. Marzani and G. P. Salam, *Towards an understanding of jet substructure*, *JHEP* **09** (2013) 029, [[1307.0007](#)].
- [10] A. J. Larkoski, S. Marzani, G. Soyez and J. Thaler, *Soft Drop*, *JHEP* **05** (2014) 146, [[1402.2657](#)].
- [11] D. Adams et al., *Towards an Understanding of the Correlations in Jet Substructure*, *Eur. Phys. J.* **C75** (2015) 409, [[1504.00679](#)].
- [12] Y.-T. Chien, A. Hornig and C. Lee, *Soft-collinear mode for jet cross sections in soft collinear effective theory*, *Phys. Rev.* **D93** (2016) 014033, [[1509.04287](#)].
- [13] A. J. Larkoski, I. Moult and D. Neill, *Analytic Boosted Boson Discrimination*, *JHEP* **05** (2016) 117, [[1507.03018](#)].
- [14] I. Moult, L. Necib and J. Thaler, *New Angles on Energy Correlation Functions*, *JHEP* **12** (2016) 153, [[1609.07483](#)].
- [15] C. Frye, A. J. Larkoski, M. D. Schwartz and K. Yan, *Precision physics with pile-up insensitive observables*, [1603.06375](#).
- [16] C. Frye, A. J. Larkoski, M. D. Schwartz and K. Yan, *Factorization for groomed jet substructure beyond the next-to-leading logarithm*, *JHEP* **07** (2016) 064, [[1603.09338](#)].
- [17] Z.-B. Kang, F. Ringer and I. Vitev, *The semi-inclusive jet function in SCET and small radius resummation for inclusive jet production*, [1606.06732](#).
- [18] Z.-B. Kang, F. Ringer and I. Vitev, *Jet substructure using semi-inclusive jet functions in SCET*, *JHEP* **11** (2016) 155, [[1606.07063](#)].
- [19] D. W. Kolodrubetz, P. Pietrulewicz, I. W. Stewart, F. J. Tackmann and W. J. Waalewijn, *Factorization for Jet Radius Logarithms in Jet Mass Spectra at the LHC*, *JHEP* **12** (2016) 054, [[1605.08038](#)].
- [20] I. Moult, L. Rothen, I. W. Stewart, F. J. Tackmann and H. X. Zhu, *Subleading Power Corrections for N -Jettiness Subtractions*, *Phys. Rev. D* **95** (2017) 074023, [[1612.00450](#)].
- [21] Y.-T. Chien and I. Vitev, *Probing the Hardest Branching within Jets in Heavy-Ion Collisions*, *Phys. Rev. Lett.* **119** (2017) 112301, [[1608.07283](#)].
- [22] I. Moult, L. Rothen, I. W. Stewart, F. J. Tackmann and H. X. Zhu, *N -jettiness subtractions for $gg \rightarrow H$ at subleading power*, *Phys. Rev. D* **97** (2018) 014013, [[1710.03227](#)].
- [23] I. Moult, B. Nachman and D. Neill, *Convolved Substructure: Analytically Decorrelating Jet Substructure Observables*, *JHEP* **05** (2018) 002, [[1710.06859](#)].
- [24] A. J. Larkoski, I. Moult and B. Nachman, *Jet Substructure at the Large Hadron Collider: A Review of Recent Advances in Theory and Machine Learning*, [1709.04464](#).
- [25] Z.-B. Kang, K. Lee, X. Liu and F. Ringer, *The groomed and ungroomed jet mass distribution for inclusive jet production at the LHC*, *JHEP* **10** (2018) 137, [[1803.03645](#)].
- [26] M. A. Ebert, I. Moult, I. W. Stewart, F. J. Tackmann, G. Vita and H. X. Zhu, *Power Corrections for N -Jettiness Subtractions at $\mathcal{O}(\alpha_s)$* , *JHEP* **12** (2018) 084, [[1807.10764](#)].
- [27] I. Moult, I. W. Stewart, G. Vita and H. X. Zhu, *First Subleading Power Resummation for Event Shapes*, *JHEP* **08** (2018) 013, [[1804.04665](#)].

- [28] Y.-T. Chien, D. Kang, K. Lee and Y. Makris, *Subtracted Cumulants: Mitigating Large Background in Jet Substructure*, *Phys. Rev. D* **100** (2019) 074030, [[1812.06977](#)].
- [29] Z.-B. Kang, K. Lee, X. Liu and F. Ringer, *Soft drop groomed jet angularities at the LHC*, *Phys. Lett. B* **793** (2019) 41–47, [[1811.06983](#)].
- [30] M. Dasgupta, F. A. Dreyer, K. Hamilton, P. F. Monni and G. P. Salam, *Logarithmic accuracy of parton showers: a fixed-order study*, *JHEP* **09** (2018) 033, [[1805.09327](#)].
- [31] R. Kogler et al., *Jet Substructure at the Large Hadron Collider: Experimental Review*, *Rev. Mod. Phys.* **91** (2019) 045003, [[1803.06991](#)].
- [32] S. Marzani, G. Soyez and M. Spannowsky, *Looking inside jets: an introduction to jet substructure and boosted-object phenomenology*, vol. 958. Springer, 2019.
- [33] A. H. Hoang, S. Mantry, A. Pathak and I. W. Stewart, *Nonperturbative Corrections to Soft Drop Jet Mass*, [1906.11843](#).
- [34] Z.-B. Kang, K. Lee, X. Liu, D. Neill and F. Ringer, *The soft drop groomed jet radius at NLL*, *JHEP* **02** (2020) 054, [[1908.01783](#)].
- [35] Y.-T. Chien, D. Y. Shao and B. Wu, *Resummation of Boson-Jet Correlation at Hadron Colliders*, *JHEP* **11** (2019) 025, [[1905.01335](#)].
- [36] Y.-T. Chien and I. W. Stewart, *Collinear Drop*, *JHEP* **06** (2020) 064, [[1907.11107](#)].
- [37] I. W. Stewart and X. Yao, *Pure Quark and Gluon Observables in Collinear Drop*, [2203.14980](#).
- [38] V. Vaidya and X. Yao, *Transverse momentum broadening of a jet in quark-gluon plasma: an open quantum system EFT*, *JHEP* **10** (2020) 024, [[2004.11403](#)].
- [39] V. Vaidya, *Effective Field Theory for jet substructure in heavy ion collisions*, *JHEP* **11** (2021) 064, [[2010.00028](#)].
- [40] J. Casalderrey-Solana, E. Shuryak and D. Teaney, *Conical flow induced by quenched QCD jets*, *J. Phys. Conf. Ser.* **27** (2005) 22–31, [[hep-ph/0411315](#)].
- [41] J. Ruppert and B. Müller, *Waking the colored plasma*, *Phys. Lett. B* **618** (2005) 123–130, [[hep-ph/0503158](#)].
- [42] A. Chaudhuri and U. Heinz, *Effect of jet quenching on the hydrodynamical evolution of QGP*, *Phys. Rev. Lett.* **97** (2006) 062301, [[nucl-th/0503028](#)].
- [43] J. Casalderrey-Solana, E. Shuryak and D. Teaney, *Hydrodynamic flow from fast particles*, [hep-ph/0602183](#).
- [44] P. M. Chesler and L. G. Yaffe, *The Wake of a quark moving through a strongly-coupled plasma*, *Phys. Rev. Lett.* **99** (2007) 152001, [[0706.0368](#)].
- [45] S. S. Gubser, S. S. Pufu and A. Yarom, *Sonic booms and diffusion wakes generated by a heavy quark in thermal AdS/CFT*, *Phys. Rev. Lett.* **100** (2008) 012301, [[0706.4307](#)].
- [46] P. M. Chesler and L. G. Yaffe, *The Stress-energy tensor of a quark moving through a strongly-coupled $N=4$ supersymmetric Yang-Mills plasma: Comparing hydrodynamics and AdS/CFT*, *Phys. Rev. D* **78** (2008) 045013, [[0712.0050](#)].
- [47] P. M. Chesler, K. Jensen and A. Karch, *Jets in strongly-coupled $N = 4$ super Yang-Mills theory*, *Phys. Rev. D* **79** (2009) 025021, [[0804.3110](#)].

- [48] P. M. Chesler, K. Jensen, A. Karch and L. G. Yaffe, *Light quark energy loss in strongly-coupled $N = 4$ supersymmetric Yang-Mills plasma*, *Phys. Rev. D* **79** (2009) 125015, [[0810.1985](#)].
- [49] R. Neufeld, B. Müller and J. Ruppert, *Sonic Mach Cones Induced by Fast Partons in a Perturbative Quark-Gluon Plasma*, *Phys. Rev. C* **78** (2008) 041901, [[0802.2254](#)].
- [50] R. Neufeld, *Mach cones in the quark-gluon plasma: Viscosity, speed of sound, and effects of finite source structure*, *Phys. Rev. C* **79** (2009) 054909, [[0807.2996](#)].
- [51] G.-Y. Qin, A. Majumder, H. Song and U. Heinz, *Energy and momentum deposited into a QCD medium by a jet shower*, *Phys. Rev. Lett.* **103** (2009) 152303, [[0903.2255](#)].
- [52] R. Neufeld and B. Müller, *The sound produced by a fast parton in the quark-gluon plasma is a 'crescendo'*, *Phys. Rev. Lett.* **103** (2009) 042301, [[0902.2950](#)].
- [53] S. S. Gubser, S. S. Pufu, F. D. Rocha and A. Yarom, *Energy loss in a strongly coupled thermal medium and the gauge-string duality*, [0902.4041](#).
- [54] P. M. Chesler, Y.-Y. Ho and K. Rajagopal, *Shining a Gluon Beam Through Quark-Gluon Plasma*, *Phys. Rev. D* **85** (2012) 126006, [[1111.1691](#)].
- [55] B. Betz, J. Noronha, G. Torrieri, M. Gyulassy and D. H. Rischke, *Universal Flow-Driven Conical Emission in Ultrarelativistic Heavy-Ion Collisions*, *Phys. Rev. Lett.* **105** (2010) 222301, [[1005.5461](#)].
- [56] A. Ayala, I. Dominguez and M. E. Tejeda-Yeomans, *Head shock vs Mach cone: Azimuthal correlations from $2 \rightarrow 3$ parton processes in relativistic heavy-ion collisions*, *Phys. Rev. C* **88** (2013) 025203, [[1212.1127](#)].
- [57] A. Ayala, J. D. Castaño Yepes, I. Dominguez and M. E. Tejeda-Yeomans, *Impact of the energy-loss spatial profile and shear-viscosity to entropy-density ratio for the Mach cone versus head-shock signals produced by a fast-moving parton in a quark-gluon plasma*, *Phys. Rev. C* **92** (2015) 024910, [[1412.5879](#)].
- [58] S. Floerchinger and K. C. Zapp, *Hydrodynamics and Jets in Dialogue*, *Eur. Phys. J. C* **74** (2014) 3189, [[1407.1782](#)].
- [59] Y. Tachibana and T. Hirano, *Momentum transport away from a jet in an expanding nuclear medium*, *Phys. Rev. C* **90** (2014) 021902, [[1402.6469](#)].
- [60] L. Yan, S. Jeon and C. Gale, *Jet-medium interaction and conformal relativistic fluid dynamics*, *Phys. Rev. C* **97** (2018) 034914, [[1707.09519](#)].
- [61] W. Chen, S. Cao, T. Luo, L.-G. Pang and X.-N. Wang, *Effects of jet-induced medium excitation in γ -hadron correlation in A+A collisions*, *Phys. Lett. B* **777** (2018) 86–90, [[1704.03648](#)].
- [62] Y. Tachibana, C. Shen and A. Majumder, *Bulk medium evolution has considerable effects on jet observables!*, [2001.08321](#).
- [63] J. Casalderrey-Solana, J. G. Milhano, D. Pablos, K. Rajagopal and X. Yao, *Jet Wake from Linearized Hydrodynamics*, *JHEP* **05** (2021) 230, [[2010.01140](#)].
- [64] J. Brewer, Q. Brodsky and K. Rajagopal, *Disentangling jet modification in jet simulations and in Z+jet data*, *JHEP* **02** (2022) 175, [[2110.13159](#)].
- [65] P. M. Chesler and K. Rajagopal, *Jet quenching in strongly coupled plasma*, *Phys. Rev. D* **90** (2014) 025033, [[1402.6756](#)].

- [66] P. M. Chesler and K. Rajagopal, *On the Evolution of Jet Energy and Opening Angle in Strongly Coupled Plasma*, *JHEP* **05** (2016) 098, [[1511.07567](#)].
- [67] J. Casalderrey-Solana, D. C. Gulhan, J. G. Milhano, D. Pablos and K. Rajagopal, *A Hybrid Strong/Weak Coupling Approach to Jet Quenching*, *JHEP* **10** (2014) 19, [[1405.3864](#)].
- [68] J. Casalderrey-Solana, D. C. Gulhan, J. G. Milhano, D. Pablos and K. Rajagopal, *Predictions for Boson-Jet Observables and Fragmentation Function Ratios from a Hybrid Strong/Weak Coupling Model for Jet Quenching*, [1508.00815](#).
- [69] J. Casalderrey-Solana, D. Gulhan, G. Milhano, D. Pablos and K. Rajagopal, *Angular Structure of Jet Quenching Within a Hybrid Strong/Weak Coupling Model*, *JHEP* **03** (2017) 135, [[1609.05842](#)].
- [70] Z. Hulcher, D. Pablos and K. Rajagopal, *Resolution Effects in the Hybrid Strong/Weak Coupling Model*, *JHEP* **03** (2018) 010, [[1707.05245](#)].
- [71] J. Casalderrey-Solana, Z. Hulcher, G. Milhano, D. Pablos and K. Rajagopal, *Simultaneous description of hadron and jet suppression in heavy-ion collisions*, *Phys. Rev. C* **99** (2019) 051901, [[1808.07386](#)].
- [72] J. Casalderrey-Solana, G. Milhano, D. Pablos and K. Rajagopal, *Modification of Jet Substructure in Heavy Ion Collisions as a Probe of the Resolution Length of Quark-Gluon Plasma*, *JHEP* **01** (2020) 044, [[1907.11248](#)].
- [73] M. Gyulassy and X.-n. Wang, *Multiple collisions and induced gluon Bremsstrahlung in QCD*, *Nucl. Phys.* **B420** (1994) 583–614, [[nucl-th/9306003](#)].
- [74] X.-N. Wang, M. Gyulassy and M. Plumer, *The LPM effect in QCD and radiative energy loss in a quark gluon plasma*, *Phys. Rev.* **D51** (1995) 3436–3446, [[hep-ph/9408344](#)].
- [75] R. Baier, Y. L. Dokshitzer, S. Peigne and D. Schiff, *Induced gluon radiation in a QCD medium*, *Phys. Lett. B* **345** (1995) 277–286, [[hep-ph/9411409](#)].
- [76] R. Baier, Y. L. Dokshitzer, A. H. Mueller, S. Peigne and D. Schiff, *Radiative energy loss of high-energy quarks and gluons in a finite volume quark - gluon plasma*, *Nucl. Phys.* **B483** (1997) 291–320, [[hep-ph/9607355](#)].
- [77] B. G. Zakharov, *Fully quantum treatment of the Landau-Pomeranchuk-Migdal effect in QED and QCD*, *JETP Lett.* **63** (1996) 952–957, [[hep-ph/9607440](#)].
- [78] R. Baier, Y. L. Dokshitzer, A. H. Mueller, S. Peigne and D. Schiff, *Radiative energy loss and $p(T)$ broadening of high-energy partons in nuclei*, *Nucl. Phys. B* **484** (1997) 265–282, [[hep-ph/9608322](#)].
- [79] M. Gyulassy, P. Levai and I. Vitev, *Jet quenching in thin quark gluon plasmas. 1. Formalism*, *Nucl. Phys. B* **571** (2000) 197–233, [[hep-ph/9907461](#)].
- [80] M. Gyulassy, P. Levai and I. Vitev, *NonAbelian energy loss at finite opacity*, *Phys.Rev.Lett.* **85** (2000) 5535–5538, [[nucl-th/0005032](#)].
- [81] U. A. Wiedemann, *Gluon radiation off hard quarks in a nuclear environment: Opacity expansion*, *Nucl. Phys.* **B588** (2000) 303–344, [[hep-ph/0005129](#)].
- [82] P. B. Arnold, G. D. Moore and L. G. Yaffe, *Photon and gluon emission in relativistic plasmas*, *JHEP* **06** (2002) 030, [[hep-ph/0204343](#)].
- [83] J. Casalderrey-Solana and E. Iancu, *Interference effects in medium-induced gluon radiation*, *JHEP* **08** (2011) 015, [[1105.1760](#)].

- [84] Y. Mehtar-Tani, C. Salgado and K. Tywoniuk, *Jets in QCD Media: From Color Coherence to Decoherence*, *Phys. Lett. B* **707** (2012) 156–159, [[1102.4317](#)].
- [85] G. Ovanessian and I. Vitev, *An effective theory for jet propagation in dense QCD matter: jet broadening and medium-induced bremsstrahlung*, *JHEP* **1106** (2011) 080, [[1103.1074](#)].
- [86] Y. Mehtar-Tani, C. A. Salgado and K. Tywoniuk, *The radiation pattern of a QCD antenna in a dilute medium*, *JHEP* **04** (2012) 064, [[1112.5031](#)].
- [87] Y. Mehtar-Tani, C. A. Salgado and K. Tywoniuk, *The Radiation pattern of a QCD antenna in a dense medium*, *JHEP* **10** (2012) 197, [[1205.5739](#)].
- [88] J.-P. Blaizot, F. Dominguez, E. Iancu and Y. Mehtar-Tani, *Medium-induced gluon branching*, *JHEP* **01** (2013) 143, [[1209.4585](#)].
- [89] J.-P. Blaizot, E. Iancu and Y. Mehtar-Tani, *Medium-induced QCD cascade: democratic branching and wave turbulence*, *Phys. Rev. Lett.* **111** (2013) 052001, [[1301.6102](#)].
- [90] J.-P. Blaizot, F. Dominguez, E. Iancu and Y. Mehtar-Tani, *Probabilistic picture for medium-induced jet evolution*, *JHEP* **06** (2014) 075, [[1311.5823](#)].
- [91] J. Ghiglieri, G. D. Moore and D. Teaney, *Jet-Medium Interactions at NLO in a Weakly-Coupled Quark-Gluon Plasma*, *JHEP* **03** (2016) 095, [[1509.07773](#)].
- [92] C. A. Salgado and U. A. Wiedemann, *Calculating quenching weights*, *Phys. Rev. D* **68** (2003) 014008, [[hep-ph/0302184](#)].
- [93] S. P. Adhya, C. A. Salgado, M. Spousta and K. Tywoniuk, *Medium-induced cascade in expanding media*, *JHEP* **07** (2020) 150, [[1911.12193](#)].
- [94] Y. Mehtar-Tani and K. Tywoniuk, *Improved opacity expansion for medium-induced parton splitting*, *JHEP* **06** (2020) 187, [[1910.02032](#)].
- [95] J. a. Barata, Y. Mehtar-Tani, A. Soto-Ontoso and K. Tywoniuk, *Medium-induced radiative kernel with the Improved Opacity Expansion*, *JHEP* **09** (2021) 153, [[2106.07402](#)].
- [96] P. Arnold, T. Gorda and S. Iqbal, *The LPM effect in sequential bremsstrahlung: nearly complete results for QCD*, *JHEP* **11** (2020) 053, [[2007.15018](#)].
- [97] P. Arnold, T. Gorda and S. Iqbal, *The LPM effect in sequential bremsstrahlung: analytic results for sub-leading (single) logarithms*, *JHEP* **04** (2022) 085, [[2112.05161](#)].
- [98] P. Arnold and O. Elgedawy, *The LPM Effect in sequential bremsstrahlung: $1/N_c^2$ corrections*, [2202.04662](#).
- [99] R. P. Feynman, *Quantum mechanical computers*, *Foundations of physics* **16** (1986) 507–531.
- [100] M. Devoret and R. Schoelkopf, *Superconducting circuits for quantum information: An outlook*, *Science (New York, N.Y.)* **339** (03, 2013) 1169–74.
- [101] M. Kjaergaard, M. E. Schwartz, J. Braumüller, P. Krantz, J. I.-J. Wang, S. Gustavsson et al., *Superconducting qubits: Current state of play*, *Annual Review of Condensed Matter Physics* **11** (2020) 369–395.
- [102] C. D. Bruzewicz, J. Chiaverini, R. McConnell and J. M. Sage, *Trapped-ion quantum computing: Progress and challenges*, *Applied Physics Reviews* **6** (2019) 021314.
- [103] F. Arute, K. Arya, R. Babbush, D. Bacon, J. C. Bardin, R. Barends et al., *Quantum supremacy using a programmable superconducting processor*, *Nature* **574** (2019) 505–510.

- [104] H. Lamm and S. Lawrence, *Simulation of Nonequilibrium Dynamics on a Quantum Computer*, *Phys. Rev. Lett.* **121** (2018) 170501, [[1806.06649](#)].
- [105] C. W. Bauer, W. A. de Jong, B. Nachman and D. Provasoli, *Quantum Algorithm for High Energy Physics Simulations*, *Phys. Rev. Lett.* **126** (2021) 062001, [[1904.03196](#)].
- [106] N. Mueller, A. Tarasov and R. Venugopalan, *Deeply inelastic scattering structure functions on a hybrid quantum computer*, *Phys. Rev. D* **102** (2020) 016007, [[1908.07051](#)].
- [107] A. Y. Wei, P. Naik, A. W. Harrow and J. Thaler, *Quantum Algorithms for Jet Clustering*, *Phys. Rev. D* **101** (2020) 094015, [[1908.08949](#)].
- [108] A. Smith, M. S. Kim, F. Pollmann and J. Knolle, *Simulating quantum many-body dynamics on a current digital quantum computer*, *npj Quantum Information* **5** (11, 2019) 106.
- [109] J. a. Barata, N. Mueller, A. Tarasov and R. Venugopalan, *Single-particle digitization strategy for quantum computation of a ϕ^4 scalar field theory*, *Phys. Rev. A* **103** (2021) 042410, [[2012.00020](#)].
- [110] A. Kan, L. Funcke, S. Kühn, L. Dellantonio, J. Zhang, J. F. Haase et al., *Investigating a $(3+1)D$ topological θ -term in the Hamiltonian formulation of lattice gauge theories for quantum and classical simulations*, *Phys. Rev. D* **104** (2021) 034504, [[2105.06019](#)].
- [111] J. M. Martyn, Z. M. Rossi, A. K. Tan and I. L. Chuang, *Grand Unification of Quantum Algorithms*, *PRX Quantum* **2** (2021) 040203, [[2105.02859](#)].
- [112] N. Klco, A. Roggero and M. J. Savage, *Standard Model Physics and the Digital Quantum Revolution: Thoughts about the Interface*, [2107.04769](#).
- [113] C. W. Bauer, M. Freytsis and B. Nachman, *Simulating Collider Physics on Quantum Computers Using Effective Field Theories*, *Phys. Rev. Lett.* **127** (2021) 212001, [[2102.05044](#)].
- [114] A. M. Czakajka, Z.-B. Kang, H. Ma and F. Zhao, *Quantum Simulation of Chiral Phase Transitions*, [2112.03944](#).
- [115] A. Ciavarella, N. Klco and M. J. Savage, *Some Conceptual Aspects of Operator Design for Quantum Simulations of Non-Abelian Lattice Gauge Theories*, **3**, 2022. [2203.11988](#).
- [116] C. W. Bauer et al., *Quantum Simulation for High Energy Physics*, [2204.03381](#).
- [117] S. P. Jordan, K. S. M. Lee and J. Preskill, *Quantum Computation of Scattering in Scalar Quantum Field Theories*, *Quant. Inf. Comput.* **14** (2014) 1014–1080, [[1112.4833](#)].
- [118] S. P. Jordan, K. S. M. Lee and J. Preskill, *Quantum Algorithms for Quantum Field Theories*, *Science* **336** (2012) 1130–1133, [[1111.3633](#)].
- [119] S. P. Jordan, H. Krovi, K. S. M. Lee and J. Preskill, *BQP-completeness of Scattering in Scalar Quantum Field Theory*, *Quantum* **2** (2018) 44, [[1703.00454](#)].
- [120] N. Klco and M. J. Savage, *Digitization of scalar fields for quantum computing*, *Phys. Rev. A* **99** (2019) 052335, [[1808.10378](#)].
- [121] S. P. Jordan, K. S. M. Lee and J. Preskill, *Quantum Algorithms for Fermionic Quantum Field Theories*, [1404.7115](#).
- [122] P. Hauke, D. Marcos, M. Dalmonte and P. Zoller, *Quantum simulation of a lattice schwinger model in a chain of trapped ions*, *Physical Review X* **3** (2013) 041018.

- [123] S. Kühn, J. I. Cirac and M.-C. Bañuls, *Quantum simulation of the schwinger model: A study of feasibility*, *Physical Review A* **90** (2014) 042305.
- [124] N. Klco, E. F. Dumitrescu, A. J. McCaskey, T. D. Morris, R. C. Pooser, M. Sanz et al., *Quantum-classical computation of Schwinger model dynamics using quantum computers*, *Phys. Rev. A* **98** (2018) 032331, [[1803.03326](#)].
- [125] T. V. Zache, N. Mueller, J. T. Schneider, F. Jendrzejewski, J. Berges and P. Hauke, *Dynamical Topological Transitions in the Massive Schwinger Model with a θ Term*, *Phys. Rev. Lett.* **122** (2019) 050403, [[1808.07885](#)].
- [126] N. Klco, J. R. Stryker and M. J. Savage, *$SU(2)$ non-Abelian gauge field theory in one dimension on digital quantum computers*, *Phys. Rev. D* **101** (2020) 074512, [[1908.06935](#)].
- [127] B. Chakraborty, M. Honda, T. Izubuchi, Y. Kikuchi and A. Tomiya, *Classically Emulated Digital Quantum Simulation of the Schwinger Model with Topological Term via Adiabatic State Preparation*, [2001.00485](#).
- [128] N. H. Nguyen, M. C. Tran, Y. Zhu, A. M. Green, C. H. Alderete, Z. Davoudi et al., *Digital Quantum Simulation of the Schwinger Model and Symmetry Protection with Trapped Ions*, *PRX Quantum* **3** (2022) 020324, [[2112.14262](#)].
- [129] W. A. de Jong, K. Lee, J. Mulligan, M. Płoskoń, F. Ringer and X. Yao, *Quantum simulation of non-equilibrium dynamics and thermalization in the Schwinger model*, [2106.08394](#).
- [130] A. Ciavarella, N. Klco and M. J. Savage, *Trailhead for quantum simulation of $SU(3)$ Yang-Mills lattice gauge theory in the local multiplet basis*, *Phys. Rev. D* **103** (2021) 094501, [[2101.10227](#)].
- [131] W. A. De Jong, M. Metcalf, J. Mulligan, M. Płoskoń, F. Ringer and X. Yao, *Quantum simulation of open quantum systems in heavy-ion collisions*, *Phys. Rev. D* **104** (2021) 051501, [[2010.03571](#)].
- [132] J. a. Barata and C. A. Salgado, *A quantum strategy to compute the jet quenching parameter \hat{q}* , *Eur. Phys. J. C* **81** (2021) 862, [[2104.04661](#)].
- [133] W. Qian, R. Basili, S. Pal, G. Luecke and J. P. Vary, *Solving hadron structures using the basis light-front quantization approach on quantum computers*, [2112.01927](#).
- [134] J. Preskill, *Quantum computing in the nisq era and beyond*, *Quantum* **2** (2018) 79.
- [135] A. He, B. Nachman, W. A. de Jong and C. W. Bauer, *Zero-noise extrapolation for quantum-gate error mitigation with identity insertions*, *Phys. Rev. A* **102** (2020) 012426, [[2003.04941](#)].
- [136] V. R. Pascuzzi, A. He, C. W. Bauer, W. A. de Jong and B. Nachman, *Computationally Efficient Zero Noise Extrapolation for Quantum Gate Error Mitigation*, *Phys. Rev. A* **105** (2022) 042406, [[2110.13338](#)].
- [137] S. J. Brodsky, H.-C. Pauli and S. S. Pinsky, *Quantum chromodynamics and other field theories on the light cone*, *Phys. Rept.* **301** (1998) 299–486, [[hep-ph/9705477](#)].
- [138] E. Farhi, J. Goldstone, S. Gutmann and M. Sipser, *Quantum computation by adiabatic evolution*, *arXiv preprint quant-ph/0001106* (2000) .
- [139] A. Alexandru, P. F. Bedaque and S. Lawrence, *Quantum algorithms for disordered physics*, *Phys. Rev. A* **101** (2020) 032325, [[1911.11117](#)].

- [140] G. H. Low and I. L. Chuang, *Optimal hamiltonian simulation by quantum signal processing*, *Physical review letters* **118** (2017) 010501.
- [141] J. M. Martyn, Y. Liu, Z. E. Chin and I. L. Chuang, *Efficient fully-coherent hamiltonian simulation*, *arXiv preprint arXiv:2110.11327* (2021) .
- [142] M. A. Nielsen and I. L. Chuang, *Quantum Computation and Quantum Information (10th Anniversary edition)*. Cambridge University Press, 2016.